The Effects of Doxorubicin Loaded Chitosan-Alginate Nanoparticles on SK-N-BE(2) Neuroblastoma Cells

Ziyaad Rahman, Student Number: 3614956

Supervisor: Professor Donavon Hiss

Co-Supervisors: Doctor Keenau Pearce & Professor Okobi Ekpo

UNIVERSITY *of the* WESTERN CAPE

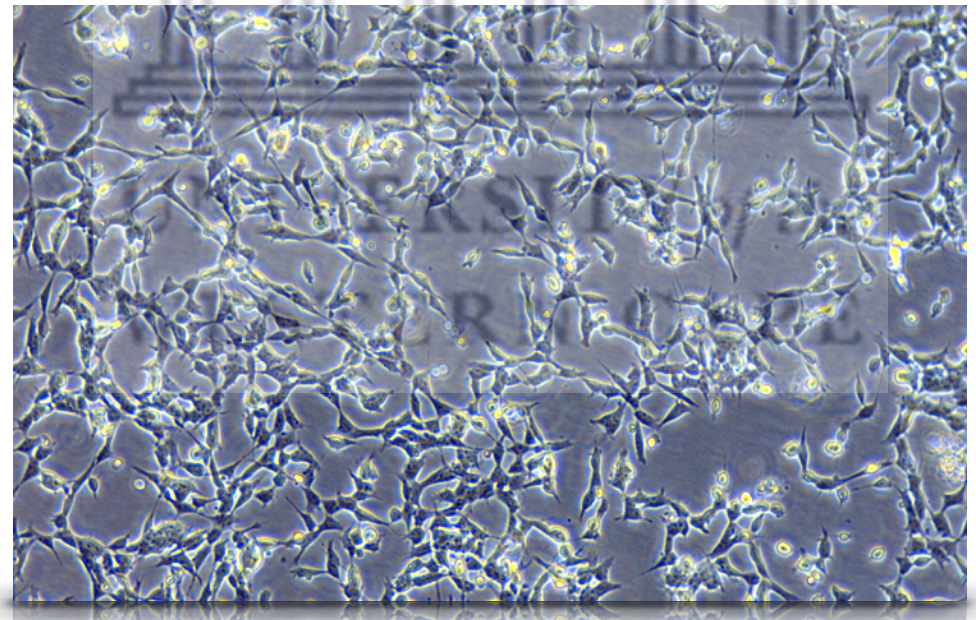

A mini-thesis submitted in partial fulfilment for the degree of Magister Scientiae (MSc) in the department of Nanoscience, University of the Western Cape, Cape Town, South Africa

28th November 2022

Declaration

I, **Ziyaad Rahman**, declare that the research study on ***"The Effects of Doxorubicin Loaded Chitosan-Alginate Nanoparticles on SK-N-BE(2) Neuroblastoma Cells"*** is my own work, that it has not been submitted for any degree or examination at any other university, that it is free of plagiarism and that all the sources used have been indicated and acknowledged by complete references.

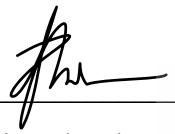

28/11/2022

Ziyaad Rahman Date

Dedication

I am dedicating this thesis to my loving wife, Alaina, who has been a constant pillar of strength for me to lean on during the many challenges of my academic journey. I am truly thankful for all the support and words of encouragement you give me daily. Your strength through everything we have been through has been my inspiration, and this journey would not have been possible without you. This work is also dedicated to my family, who have continuously supported me and believed in the things I aspire to achieve.

Success is not final;

Failure is not fatal;

It is the courage to continue that counts.

Acknowledgements

Firstly, I would like to thank God The Almighty for granting me the opportunity, strength, wisdom and guidance in everything I do. Without firm trust in Him it would not have been possible for me to come this far.

I would like to thank my parents for the love and immeasurable amount support they have shown me through these challenging years. For the patience and comfort they have given me in times when I needed it most.

To my supervisors, Professor Donavon Hiss and Professor Okobi Ekpo, thank you for believing in me, remaining committed to this research and inspiring me to think outside the box. Thank you for all the help during the course of my degree, and for the insightful conversations every time we met.

To my co-supervisor, Doctor Keenau Pearce, I have the utmost gratitude for your patience with me and your ever helpful personality. It was something that could be rivalled by very few. Without your help, this project would have definitely been a lot more challenging. To Andrea Hendricks, Tusekile Kangwa and all my other senior colleagues, you turned one of the most challenging experiences in my university career into one of the best and most memorable.

I would also like to express my gratitude to the lecturers in the Medical Bioscience department, the knowledge I have gained throughout the years will be something I cherish for the rest of my life. To my work study co-ordinator, Mrs Marjorie Smith, thank you for your patience, and allowing me the opportunity to gain experience and knowledge from you throughout this year. To Mr Braaf, it was a pleasure working with you, and assisting in practicals during the course of my work-study journey. I have definitely gained a friend in you.

Last but certainly not least, to my closest friend throughout my university career Joshua Delport, thank you for all the motivation, assistance, endless amounts of laughter and memories we made throughout the years.

Abstract

Cancer is a life-threatening disease and one of the leading causes of death globally. Cancer was thought to be associated with developed countries only but it is increasingly becoming a major health challenge in developing countries, including South Africa. Neuroblastoma is a form of cancer that affects the very early forms of nerve cells and is the most common extra-cranial solid tumour in children. It develops mainly in the adrenal medulla and the sympathetic ganglia. The focus of the present study is the development of a doxorubicin-loaded nanoparticle drug delivery system for the treatment of neuroblastoma. The biological diversity of the neuroblastic tumours that occur in patients has led to a divided approach in therapeutic strategies. Recent research efforts are aimed at designing therapies that will exploit the key oncogenic features of tumours, either within the tumours, in the tumour microenvironment, or both. Although doxorubicin chemotherapy is known to be generally very effective, previous studies have shown that it may result in the undesired toxicity of cardiomyocytes, cardiac fibroblasts, cardiac progenitor cells, endothelial progenitor cells, smooth muscle cells, and mesenchymal stem cells.

To minimize the toxic effects caused by doxorubicin, nanocarrier drug delivery systems could be developed to decrease the doses of this drug administered whilst maintaining its efficacy. In the present study, doxorubicin was encapsulated in chitosan-alginate nanoparticles synthesized by ionotropic gelation. The average size of the synthesized nanoparticles was 361nm, with a calculated polydispersity index of 0.260, and a zeta potential of -39.6 mV. The IC50 concentrations that were tested and confirmed following 24 and 48-hour exposure to doxorubicin had encapsulation efficiencies of 86% and 66% respectively. The SK-N-BE(2) neuroblastoma cells were exposed to the unloaded nanoparticles as well as the doxorubicin-loaded nanoparticles at log10 concentrations for 24 and 48 hours, after which cell morphology was examined via light microscopy, and cell viability graphs and dose-response curves were obtained from the absorbance readings of MTT assays. In addition, the levels of reactive oxygen species (ROS) produced following nanoparticle exposure were also quantified.

The results obtained showed that there were no significant decreases in cell viability, and no changes in morphology were observed following exposure to the various nanoparticle formulations over both time points. Also, there were no significant increases in the production of ROS. These

results tend to suggest that although treatment with the doxorubicin nanoparticles was effective in killing the cancer cells, significant biocompatibility was demonstrated. The results of this study generally align with the current global trends that focus on the analysis of *in vitro* drug effects elicited by nanoparticle drug delivery systems and various target treatments. Future studies could build on the data obtained from the current study by evaluating the release of doxorubicin from the nanoparticle system, increasing its efficacy through the incorporation of drug combinations, and functionalization of the nanoparticles to improve their biological activities.

Key words: childhood cancer, neuroblastoma, doxorubicin, nanoparticle delivery system, chitosan, alginate, drug encapsulation, cytotoxicity, biocompatability, viability, apoptosis, reactive oxygen species

Contents

List of Abbreviations

^{131}I-MIBG - Iodine-131 metaiodobenzylguanidine

AA - Acetic acid

AGn - Arabipogalactan

ALG - Alginate

ALK - Anapaestic lymphoma kinase

BSA - Bovine serum albumin

CHS - Central hypoventilation syndrome

CNT - Carbon nanotubes

CS - Chitosan

CS-ALG - Chitosan-alginate

CT - Computed tomography

dH_2O - Distilled water

DLS - Dynamic light scattering

DNA - Deoxyribonucleic acid

DWNT - Double walled carbon nanotubes

DX-CS-ALG - Doxorubicin loaded chitosan-alginate

EPR - Enhanced Permeability and Retention

EPR - Enhanced permeability and retention effect

FDG-PET - [18 F]-fluorodeoxyglucose positron emission tomography

HB - Hepatoblastoma

IDRFs - Image-defined risk factors

INRGSS - International Neuroblastoma Risk Group Staging System

INSS - International Neuroblastoma Staging System

IRE - Iron regulatory proteins

LbL - Layer-by-layer Assembly

LDH - Lactate dehydrogenase

MIBG - Meta-iodobenzylguanidine

MRI - Magnetic resonance imaging

MTT - 3-(4,5-Dimethylthiazol-2-yl)-2,5-Diphenyltetrazolium Bromide

MWNT - Multi-walled carbon nanotubes

NP - Nanoparticle

NP-Dox-Curcumin - Nanoparticle-doxorubicin-curcumin complex

PDI - Polydispersity Index

PEG - Polyethylene glycol

PEG-Dox - Pegylated doxorubicin conjugate

PEI - Polyethylenimine

PLL - Poly-L-lysine

PMC - Polyelectrolyte Multilayer Capsules

PS - Monodisperse Polystyrene nanoparticles

Pul - Pullanan

RNA - Ribonucleic acid

ROS - Reactive oxygen species

RyR2 - Rynodine receptor

SERCA2A - Ca^{2+} ATPase of sarco/endoplasmic reticulum

SWNT - Single walled carbon nanotubes

TAT - Tat peptide

TEM - Transmission electron microscopy

TPP - Tripolyphosphate

List of Figures

List of Tables

Chapter 1
Literature Review & Introduction

1.1 Cancer

Cancer is a life-threatening disease that has become one of the worlds leading killers. This disease is considered to be a disease of the cell, brought upon by mutations in genes that govern cell growth, death, metabolism, and repair. In all various forms of cancer, the body's cells begin to divide uncontrollably and spread into surrounding tissues (National Cancer Institute, 2019). Hanahan and Weinberg have proposed 8 biological hallmarks that describe key orogenic features, which have proved useful in understanding cancer at a cellular level (Hanahan and Weinberg, 2011). However, recently the tumor microenvironment is thought to be a co-conspirator in tumor cell initiation and progression. As cancer progresses, tumor cells disrupt tissues surrounding them biochemically and physically, whilst simultaneously recruiting healthy cells, causing further alterations in the matrix and cellular composition of tumors. Therefore, in addition to the 8 hallmarks described by Hanahan and Weinberg in 2011, Nia, Munn and Jain have proposed 4 additional features stemming from physical abnormalities of tumors. These features are increased solid stress, increased interstitial fluid pressure, increased stiffness with changed material properties, and altered microarchitecture (Nia, Munn and Jain, 2020).

Figure 1 illustrates how the physical interactions of cancer cells with stroma give rise to the physical features of tumor cells through distinct and interconnected mechanisms. For instance, compressed and leaky blood vessels in combination with nonfunctional lymphatics lead to increased fluid pressure within tumors (Chauhan et al., 2014). In addition, cellular proliferation, matrix deposition, and cell contraction coupled with abnormal growth patterns gives rise to compressive, tense solid stresses. Similarly, these traits are able to alter the microarchitecture of tissue (Seano et al., 2019). Lastly, the physical hallmarks highlighted are also able to interact with each other causing one or more of the other hallmarks. The tumor microenvironment is thus anomalous both physically and biologically, leading to an increased appreciation to the role it plays in cancer. Consequently this has led to numerous discoveries about the origins and consequences of these physical traits, which has ultimately resulted in new targeted treatment strategies for patients. Whilst it may seem that these physical traits are specific to solid cancers, there is increasing

evidence that they may also contribute to the treatment strategies and progression of haematological cancers (Nia, Munn and Jain, 2020).

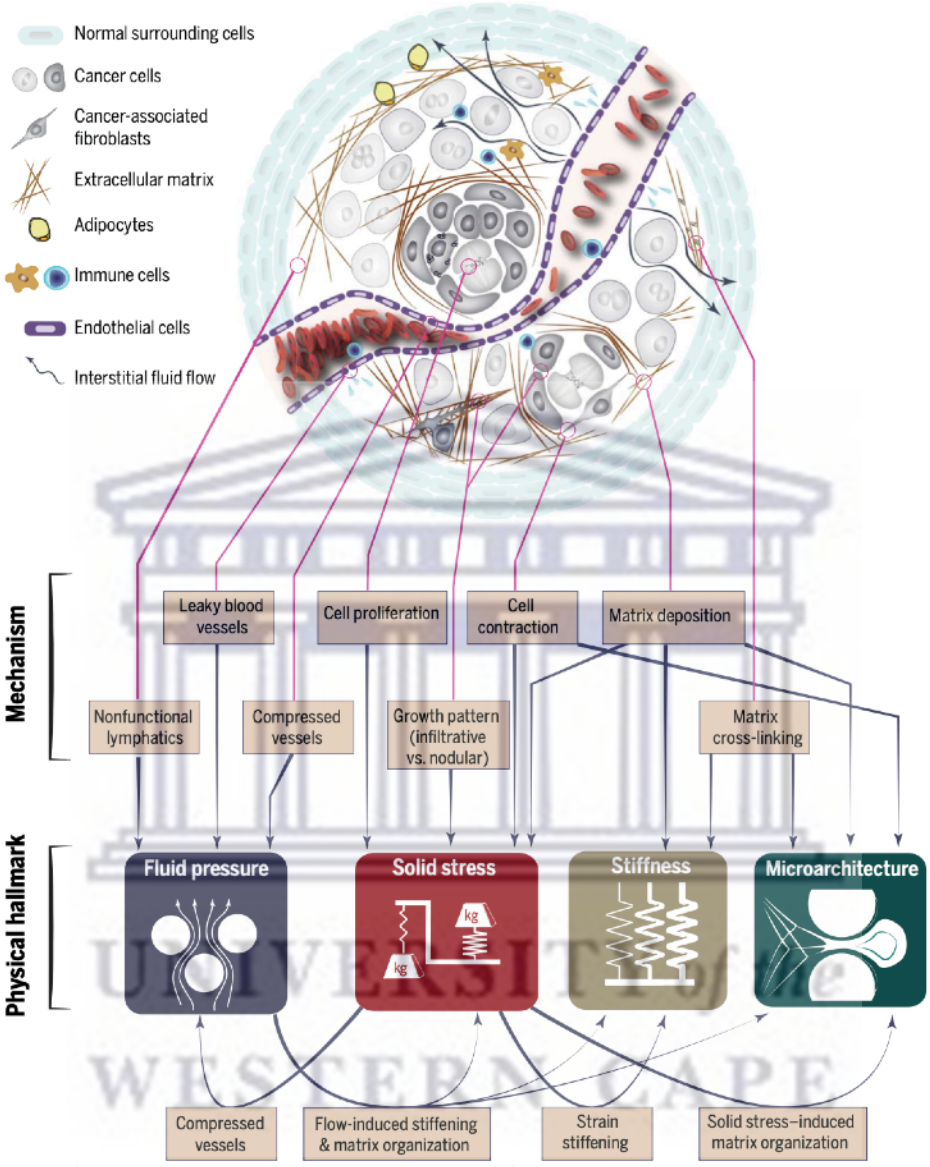

Figure 1: Origins of the physical traits of cancer (Nia, Munn and Jain, 2020)

Cancer is not only a major killer in first-world countries, but has become an increasing burden in developing countries including South Africa (Jemal et al., 2012). The increased burden of cancer in these developing nations is a result of population ageing and growth, but also increasing adaptation to cancer-associated lifestyle choices such as physical inactivity and western diets often associated with first-world countries (Pilleron et al., 2019). In 2018, 752 000 new cancer cases and 506 000 cancer deaths were documented in Sub-Saharan Africa, with cervical, breast, and prostate cancer as

the most prevalent. For example, in Zimbabwe and Uganda, breast cancer cases are rapidly increasing with an average annual percentage of 4.9% and 4.5% respectively between 1991 and 2010 (Joko-Fru et al., 2020). It is due to alarming statistics such as these that epidemiologists suggest that cancer incidence and burden in Sub-Saharan Africa will more than double in 20 years (Munung, Ambele and Moela, 2021).

1.2 Neuroblastoma

Neuroblastoma is the most common extra-cranial solid tumor in children, that develops mainly in the adrenal medulla as well as the sympathetic ganglia (Tsubota and Kadomatsu, 2017). Based on these common sites of primary disease as well as the cellular and neurochemical features, it is widely accepted that this type of cancer originates from the sympathoadrenal lineage of neural crest cells during development (Cheung and Dyer, 2013). Put simply, neuroblastoma is cancer of very early forms of nerve cells (Cancer.org, 2019). Under ideal circumstances, neural crest cell precursors migrate from the dorsal neural tube and differentiate once they arrive at their appropriate location in tissues and organs of the sympathetic nervous system. Figure 2 illustrates the anomalies in the migration, maturation, and differentiation of these neural crest cells leading to the development of neuroblastoma (Whittle et al., 2017).

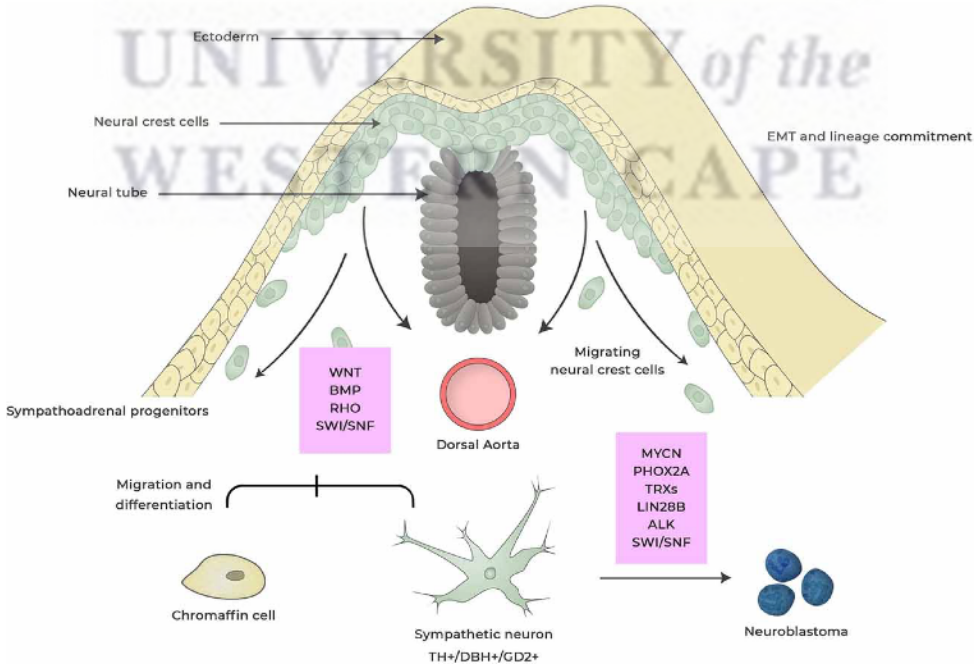

Figure 2: Development of neuroblastoma from neural crest cells (Johnsen, Dyberg and Wickström, 2019)

Neuroblastoma accounts for approximately 10% of all childhood cancers, whilst its prevalence is roughly 1 case per 7000 live births (Forouzan-Moghaddam et al., 2018). Currently, neuroblastoma is the primary cause of death for children suffering from paediatric cancer between the age of 1-5 years and in total accounts for approximately 15% of all paediatric cancer deaths (Louis and Shohet, 2015; Whittle et al., 2017). Approximately half of neuroblastoma patients have an abject outcome despite intensive multimodal treatments, whilst some patients have outstanding outcomes due to their tumors spontaneously regressing or differentiating into benign ganglioneuromas (Ackermann et al., 2018).

Neuroblastoma exhibits extremely different clinical phenotypes, such as spontaneous regression but also aggressive growth. This type of different biological behaviour appears to be determined by genetic abnormalities such as MYCN oncogene amplification, DNA ploidy and allelic imbalances (Nakagawara, 2004). According to the Children's Oncology Group, the 5-year survival rate of neuroblastoma patients is divided into 3 main categories, namely; low-risk, intermediate-risk, and high-risk. Patients in the high-risk group have a 5-year survival rate of approximately 50%, whilst those in the intermediate and low-risk groups have a 5-year survival rate of 90% and 95% respectively (Neuroblastoma Survival Rates | American Cancer Society, 2022). Outcomes in patients that suffer from this disease have improved, with 5-year survival rates increasing from 52% between 1975 to 1977 to 74% between 1999 to 2005. This improvement is mainly attributed to increased cure rates in patients suffering from the more benign form of the disease. Those that suffer from the more high-risk neuroblastoma have only shown modest improvements despite the dramatic escalation in the intensity of the provided therapies (Maris, 2010). Figure 3 illustrates the difference between the overall 5-year survival for all cancer patients compared to neuroblastoma.

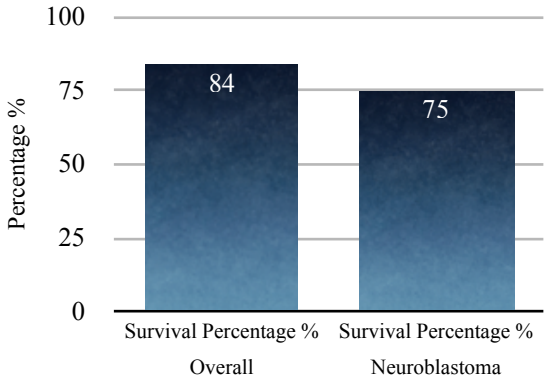

Figure 3: Five-year survival rate for overall cancer patients compared to neuroblastoma patients (Visualsonline.cancer.gov, 2019)

1.2.1 Genetics of Neuroblastoma

The incidence of neuroblastoma is roughly 10.5 cases per million children under the age of 15 years in North America and Europe, with little ethnic and geographic variability. However, it is diagnosed slightly more in boys than girls. African American and Native American patients have been known to suffer from more aggressive forms of the disease with lower rates of survival, although the aetiology of these differences is unclear (Henderson et al., 2011). The fundamental aetiology of most neuroblastic tumors remains unknown, and although environmental factors have been suggested as possible causes, a direct link has not been established (Whittle et al., 2017).

Most neuroblastoma tumors occur as isolated incidents in families, suggesting that the rates of oncogenic germline mutations are low. This is evident as approximately 1% - 2% of all cases of neuroblastoma are associated with a positive family history (Shojaei-Brosseau et al., 2003). Neuroblastoma has also been known to occur in patients suffering from Hirschsprung disease and central hypoventilation syndrome (CHS), and whilst the underlying aetiology of the associations is unclear, mutations in the PHOX2B gene present in both diseases are also detected in familial neuroblastoma. Large-scale genetic studies performed in families with familial neuroblastoma have identified numerous other chromosomal susceptibility regions, including 2p23-26, 12p, and 16p. This has subsequently led to the discovery of germline mutations in the anapaestic lymphoma kinase (ALK) gene. Majority of patients suffering from familial neuroblastoma have germline mutations in ALK, with sporadic neuroblastoma tumors also harbouring ALK abnormalities (Mossé et al., 2008).

Genome-wide association studies have also identified supplementary germline genetic variations in neuroblastoma, including single nucleotide polymorphisms in BARD1, LMO1, and LIN28B, amongst others. Furthermore, other polymorphisms in other chromosomal regions have yet to be fully characterised. These polymorphisms occur quite frequently in the general population and may contribute to the development of sporadic neuroblastoma, but the functional roles of these germline variations in addition to other somatic alterations still need to be fully explained (Whittle et al., 2017).

1.2.2 Clinical Presentations and Diagnosis of Neuroblastoma

This type of cancer is often referred to as an "enigmatic tumor" due to its broad spectrum of clinical and biological features (Malis, 2013). Tumors for this disease can arise anywhere along the sympathetic nervous system, but the majority occur in the adrenal medulla, followed by abdominal, cervical, thoracic and pelvic sympathetic ganglia. Primary tumors that present in the neck or upper areas of the chest can cause Horners Syndrome, whilst tumors that present along the spinal column can expand through the intraforaminal spaces and compress the spinal cord resulting in paralysis (Maris, 2010). Additionally, tumors metastasise to lymph nodes, bone marrow, bones, liver, and skin, but rarely to the lungs and brain. Widespread bone and bone marrow disease may cause bone pain which can lead to limping and severe irritability. Skin involvement is observed almost exclusively in children with stage 4S tumors, and is characterised by a variable number of contender, bluish subcutaneous nodules. With this type of cancer, many lower-stage tumors are encapsulated and can be surgically removed with a very low chance of complications. On the other hand, higher-stage tumors often infiltrate local organ structures, surround vital nerves and are usually unresectable at the time of diagnosis (Maris, 2010). Some of the common clinical presentations discussed are shown in Figure 4.

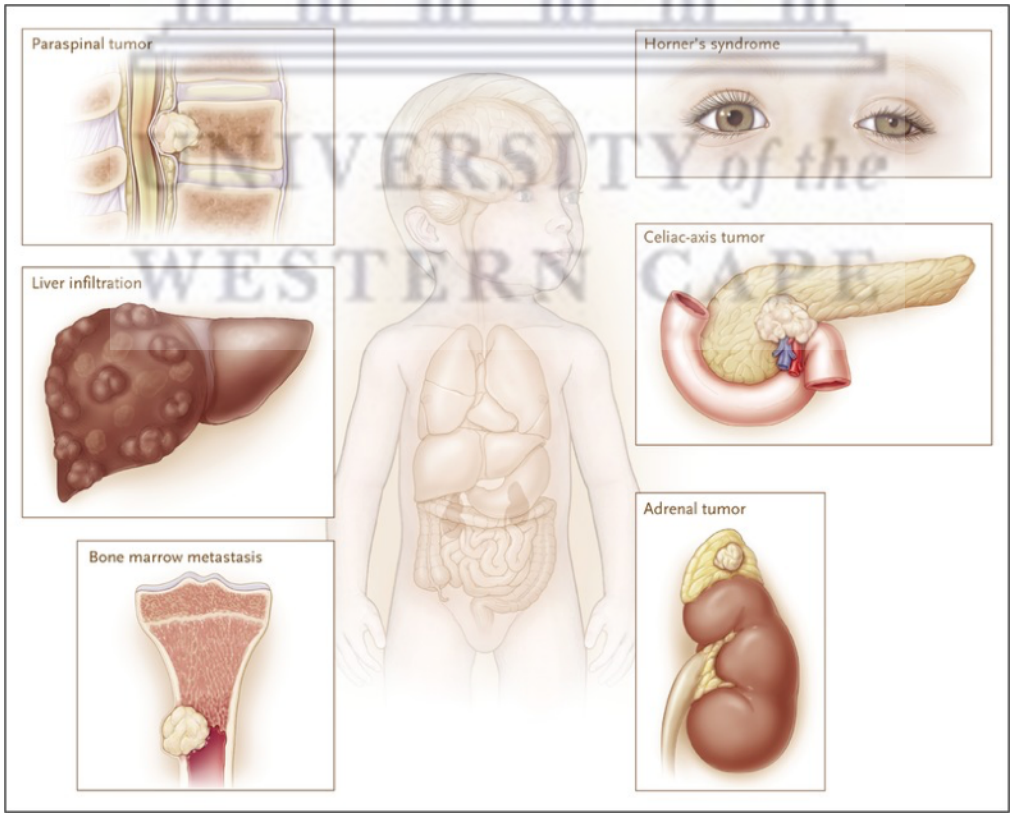

Figure 4: Common clinical presentations of neuroblastoma (Maris, 2010)

The assessment to decide the disease stage in children presenting with neuroblastoma commonly includes imaging of the primary tumor site with computed tomography (CT) or magnetic resonance imaging (MRI). This helps determine primary tumor size as well as the regional invasion and spread (Whittle et al., 2017). Additionally, meta-iodobenzylguanidine (MIBG) scans can be used to detect primary tumors and metastatic sites, with roughly 90% of patients having MIBG-avid tumors. On the other hand, patients who do not have MIBG-avid tumors use [18 F]-fluorodeoxyglucose positron emission tomography (FDG-PET) (Bleeker et al., 2015). In addition to imaging tests, bone marrow aspirates and tissue biopsies from at least two independent sites are obtained. Ultimately, diagnosis of neuroblastoma can be confirmed either by imaging tests in conjunction with tumor tissue biopsies using histopathology, or by the combination of elevated urine or serum catecholamine levels (Whittle et al., 2017).

1.2.3 Staging of Neuroblastoma

Staging is a way of describing cancer. It can tell us where it is located, whether it has spread or whether it is affecting other parts of the body. This can then help a physician decide on the best course of treatment. The INSS (International Neuroblastoma Staging System) was the first internationally accepted staging system and was developed in 1988. In 2009, the INRG (International Neuroblastoma Risk Group) task force proposed a new system (the International Neuroblastoma Risk Group Staging System - INRGSS) that was based on imaging technology (Malis, 2013). One of the pros associated with the INRGSS is its utilisation of image-defined risk

Table 1: International Neuroblastoma Risk Group Staging System. Adapted from the American Cancer Society (http://www.cancer.org/)

International Neuroblastoma Risk Group Staging System (INRGSS)	
L1	The tumor has not spread from its origin and has not spread into vital structures as defined by the list of IDRFs. It is confined to one part of the body
L2	The tumor has not spread far from where it originated and has at least one IDRF
M	The tumor has spread to a distant part of the body but does not meet the MS criteria
MS	Metastatic disease in patients younger than 18 months with cancer spread to only the skin, liver, and/or bone marrow

factors (IDRFs) to determine the best course of treatment and how resectable the tumor may be. Tables 1 and 2 describing the two staging systems are shown below.

Table 2: International Neuroblastoma Staging System. Adapted from the American Cancer Society (http://www.cancer.org/)

International Neuroblastoma Staging System (INSS)	
Stage 1	Localised tumor on one side of the body that has been completely removed by surgery. Lymph nodes near the tumor are free of cancer.
Stage 2A	Localised tumor on one side of the body, however not all has been removed by surgery. Lymph nodes near the tumor are free of cancer.
Stage 2B	Localised tumor on one side of the body that has not been completely removed by surgery. Nearby lymph nodes outside the tumor contain neuroblastoma cells, however cancer has not spread to the other side of the body or elsewhere.
Stage 3	Unresectable unilateral tumor infiltrating across the midline, with or without regional lymph node involvement; or a localised tumor with contralateral regional lymph node involvement; or a midline tumor that may be spreading to both sides of the body.
Stage 4	The cancer has spread to distant parts of the body, however he patient does not meet the criteria for stage 4S
Stage 4S	The patient is younger than 1 year old. Localised tumor with dissemination limited to the liver, skin and/or bone marrow.

1.2.4 Treatment of Neuroblastoma

The biological diversity of neuroblastic tumors that occur in patients has led to a divided approach in therapeutic strategies. For tumors that have favourable biologic features, the trend leans towards reducing the therapeutic intensity. In contrast, the approach to tumors with adverse prognostic features has shifted towards intensifying chemoradiotherapy. Recent research is aimed at attempting to design therapies that will exploit key oncogenic features found in the tumor itself, or in the tumor microenvironment, or both (Maris, 2010).

In North America, the majority of patients are treated using guidelines set up by the Children's Oncology Group. Using results obtained from more than 2 decades of clinical trials, the group has developed a risk group stratification that combines the use of INSS/INRGSS staging with the age at diagnosis, histological results, and the biology and genetics of the tumor to place patients into a low-, intermediate-, or high-risk group. The intensity and duration of treatment is then determined (Swift, Eklund, Kraveka and Alazraki, 2018). Patients who fall into the low-risk group often receive surgery to resect tumors, however, studies in North America and Europe suggest that complete surgical resection for low- to intermediate-risk tumors is not necessary (Baker et al., 2010) (De Bernardi et al., 2008). For low-risk tumors that are in locations where surgery is not possible, such as tumors causing spinal cord compression or respiratory compromise, chemotherapy is used. Additionally, patients with intermediate-risk tumors receive chemotherapy to shrink tumors before surgical resection is carried out. Radiation therapy is rarely indicated for patients with intermediate-risk tumors, but should be considered when tumors progress or there are life-threatening complications associated with chemotherapy (Swift, Eklund, Kraveka and Alazraki, 2018). Patients who suffer from high-risk tumors use an aggressive multimodal approach, which includes neoadjuvant chemotherapy, surgical resection, adjuvant high dose chemotherapy with hematopoietic stem cell rescue and radiation therapy (Laprie et al., 2004).

Targeted approaches for neuroblastoma may revolutionise the way in which this diseases is treated and managed. Iodine-131 metaiodobenzylguanidine (^{131}I-MIBG) treatment allows for a targeted approach to treating neuroblastoma. It is a new technique that patients tend to respond more favourably to as it does not cause adverse side effects such as nausea and pain. Additionally, this type of treatment is known to provide palliative relief from pain caused by metastatic bone disease and other neuroendocrine tumors (Gedik, Hoefnagel, Bais and Valdés Olmos, 2008). However, clinical trials are underway to investigate its use as a primary and adjuvant therapy (Swift, Eklund, Kraveka and Alazraki, 2018).

1.2.5 Prognostic Markers for Neuroblastoma

Prognostic markers are features that help predict whether a patients outlook for cure is better or worse than would be predicted by the stage alone. These markers are used in combination with the patients stage to assign them to a risk group. Markers used to determine the prognosis of patients are presented in Table 3.

Table 3: Prognostic markers for neuroblastoma. Adapted from the American Cancer Society (http://www.cancer.org/)

Prognostic Markers	
Age	Younger patients (under 12-18 months) are more likely to have a favourable outcome compared to older patients.
Tumor histology	Tumors that contain more normal-looking cells and tissues tend to have a more favourable prognosis and histology.
DNA ploidy	The amount of DNA in each cells can be measured using specialised lab tests. Neuroblastoma cells with a similar amount of DNA as normal cells are classified as diploid, whilst those with more DNA are classified as hyperdiploid. Neuroblastoma cells with more DNA are associated with a better prognosis, particularly in younger patients (under 2 years).
MYCN gene amplification	Alterations in the MYCN gene can turn it into an oncogene, which in turn can make cells divide and grow faster. Neuroblastomas with MYCN amplification tend to grow quick and prove difficult to treat.
Chromosome alterations	Tumor cells that exhibit 1p and 11q deletions may predict a less favourable prognosis. Similarly, cells showing 17q gains are linked to a worse prognosis. Thus, understanding chromosome deletions and gains has become an increasingly active area of neuroblastoma research
Neurotrophin (nerve growth factor) receptors	These substances are present on the surface of normal nerve cells and some neuroblastoma cells. Under normal conditions, these receptors allow cells recognise neurotrophins, which are hormone-like chemicals that help nerve cells mature. Neuroblastomas that contain more of a specific neurotrophin receptor, particularly nerve growth factor receptor TrkA, may have a more favourable prognosis.
Serum markers	Neuroblastoma cells are known to release **ferritin** into the blood, a chemical that is an important part of iron metabolism. Patients with high ferritin levels tend to have worse prognosis. Increased levels of **lactate dehydrogenase (LDH)** are also linked with a worse prognosis in patients.

1.3 Chemotherapy

The development of cytotoxic chemotherapy dates back as far as the First World War, when soldiers who were treated for the irritant effects of sulphur mustard gas were known to develop lymphoid aplasia. These nitrogen mustards were the first chemical agents to undergo clinical studies and consequently produced dramatic regressions in lymphoma patients (Corrie, 2008). Infact, most of the cytotoxic anti-cancer drugs in use currently have been shown to induce apoptosis in susceptible cells. The fact that contrasting agents, which interact with different targets induce cell death with some common features suggests that cytotoxicity is determined by the ability of the cell to engage this so-called "programmed" cell death (Hickman, 1992).

The ability of chemotherapy to kill cancer cells depends on its ability to halt cell division. Usually, the drugs work by damaging the RNA or DNA that tells the cell how to replicate and divide. Thus, if they are unable to divide, they die. Generally, chemotherapy agents are divided into two groups. Chemotherapy drugs that affect cells only when they are dividing are called cell-cycle specific (plant alkaloids and antimetabolites), whilst those that only affect cells when they are at rest are called cell-cycle non-specific (alkylating agents and some natural products) (see Table 4). It is common to follow a therapy that involves the use of cell cycle non-specific drugs in combination with cell-cycle specific drugs, so that the cancer cells are recruited into the cell cycle where the drug can be most effective. Finally, The scheduling of chemotherapy is set based on the type of cells, the rate at which they divide, and the time at which a given drug is likely to be effective. This is why chemotherapy is typically given in cycles (Cancer, 2019).

Table 4: Differences between cell cycle specific and cell cycle non-specific drugs (Fitzakerly, 2022).

Cell Cycle Specific	Cell Cycle Non-Specific
Primary action only during specific phases of the cell cycle. • Plant alkaloids: G_2-M phase • DNA synthesis inhibitors: S phase	Primary action occurs during any phase, including G0, however the final toxicity may be manifested during a specific phase. • Crosslinking agents • Anthracycline antibiotics
Only proliferating cells are killed (high growth factor tumors are preferentially targeted).	Both proliferating and non-proliferating cells are killed (both high and low growth factor tumors are targeted)
Schedule dependant (duration and timing matter in addition to the dose of the drug).	Dose dependant (total dose matters more than the schedule)

1.3.1 Clinical Applications of Chemotherapy

By virtue of their high proliferative index, many haematological malignancies initially respond well to chemotherapy. High grade leukemias and lymphomas can be cured with aggressive treatment strategies, whilst lower grade tumors can be effectively managed over many years with drug doses suited to allow activities associated with daily living. However, if a patient has to relapse the prognosis is less favourable and re-treatment may not achieve durable remission (Corrie, 2008).

Surgery and radiotherapy are the principal modalities used in the treatment of localised solid cancers. However, many patients present with metastatic spread, or develop recurrent disease at the primary site or distant sites that can not be accessed by these means. Cytotoxic chemotherapy is usually offered to patients with advanced disease, but it is rarely curative. The best response to chemotherapy is typically a decrease in tumor volume, which may provide a significant effect in terms of duration of survival and symptom control compared to the natural course of the disease (Corrie, 2008).

1.3.2 Limitations and Drawbacks to Chemotherapy

One of the most common reasons for treatment failure is drug resistance acquired through intrinsic and acquired mutations in tumorigensis, which ultimately protects the cancer cells from chemotherapy (Corrie, 2008). Additionally, chemotherapy is associated with various severe side effects, which include instantaneous signs of toxicity and late signs of chronic toxicity. According to The World Health Organisation, their intensity can be mild (grade 1), moderate (grade 2), severe (grade 3), or life-threatening (grade 4) (Schirrmacher, 2019). Some immediate side effects associated with chemotherapy include myelosuppression, nausea, vomiting, hair loss and reduced fertility. However, numerous men and women are able to recover their fertility, but this depends on the patients age, the type and total dose of the drugs received, and the time-off treatment. Furthermore, most cytotoxic agents are teratogenic and potentially harmful to the foetus. Therefore patients receiving chemotherapy are counselled to use appropriate contraception for the duration of their respective treatment. Lastly, some chronic side effects associated with chemotherapy include cardiomyopathy induced by doxorubicin, and pulmonary fibrosis associated with bleomycin. To avoid such side effects, checks have been established to limit the amount of drug that can be prescribed over time (Corrie, 2008). Furthermore, efforts to mitigate doxorubicin cardiomyopathy and other adverse effects have been undertaken via liposomal drug delivery (Zhao, Woodle and Mixson, 2018).

1.3.3 Doxorubicin

Doxorubicin is a type of chemotherapy drug called an anthracycline (Cancerresearchuk.org, 2019). It may be used alone or in combination with other chemotherapy agents, and is a common first-line therapy for numerous cancers including breast, ovarian, bladder, and lung cancer (Zhao, Woodle and Mixson, 2018). In 1991 Ortega et al. demonstrated how using doxorubicin in combination with other drugs produced a successful therapy leading to surgical resectabilty in children with hepatoblastoma (HB), thus making long-term survival an obtainable goal for patients with unresectable tumors. Whilst the mechanism of action for doxorubicin is still being studied, proposed mechanisms include DNA intercalation causing disruption in gene expression, reactive oxygen species (ROS) generation, and inhibition of topoisomerase II, a gyrase important for DNA synthesis and replication (Zhao, Woodle and Mixson, 2018). Lately, Denard et al. found that doxorubicin increased intracellular ceramide levels, ultimately resulting in the release of a membrane transcription factor, CREB3L1. This transcription factor affects the expression of multiple genes, notably p21, which is a tumor suppressor. Interestingly, cells with elevated CREB3L1 levels are significantly more sensitive to doxorubicin than those with lower levels (Denard, Jiang, Peng and Ye, 2018).

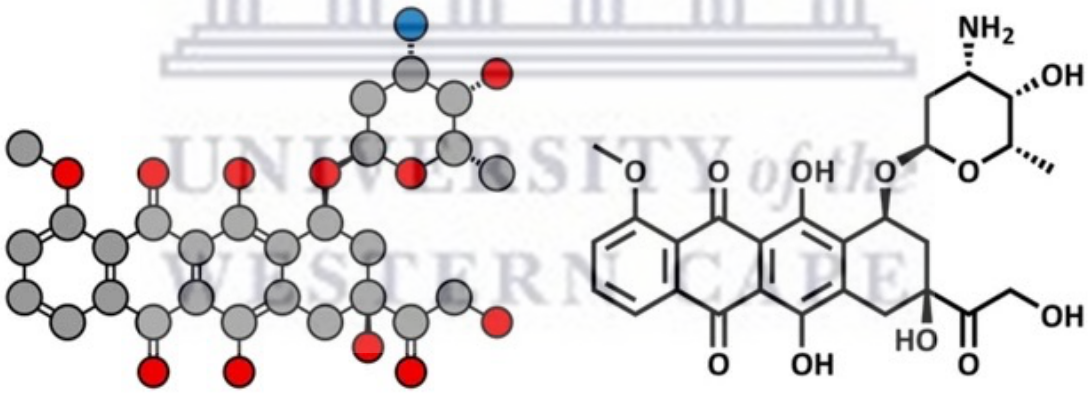

Figure 5: Structural formula of doxorubicin

Despite all the proposed mechanisms of action, doxorubicin definitively has cell cycle-specific activity. In addition to causing G_0/S and G_2/M arrest, it also results in the increase of ROS leading to apoptosis. Additionally, doxorubicin has p53 dependent and independent mechanisms. Interestingly, the delivery method may influence the pathway activated by doxorubicin. For instance, bolus injection results in significant apoptosis of treated cells associated with G_2 arrest, p53 phosphorylation, and increased levels of p21 and BAX. Dissimilarly, cells exposed to constant

levels of doxorubicin show a decrease in cell number but very little apoptosis (Zhao, Woodle and Mixson, 2018). The cellular entry of doxorubicin usually occurs through rapid diffusion and carrier-mediated uptake, strongly dependent on temperature and pH (Sritharan and Sivalingam, 2021).

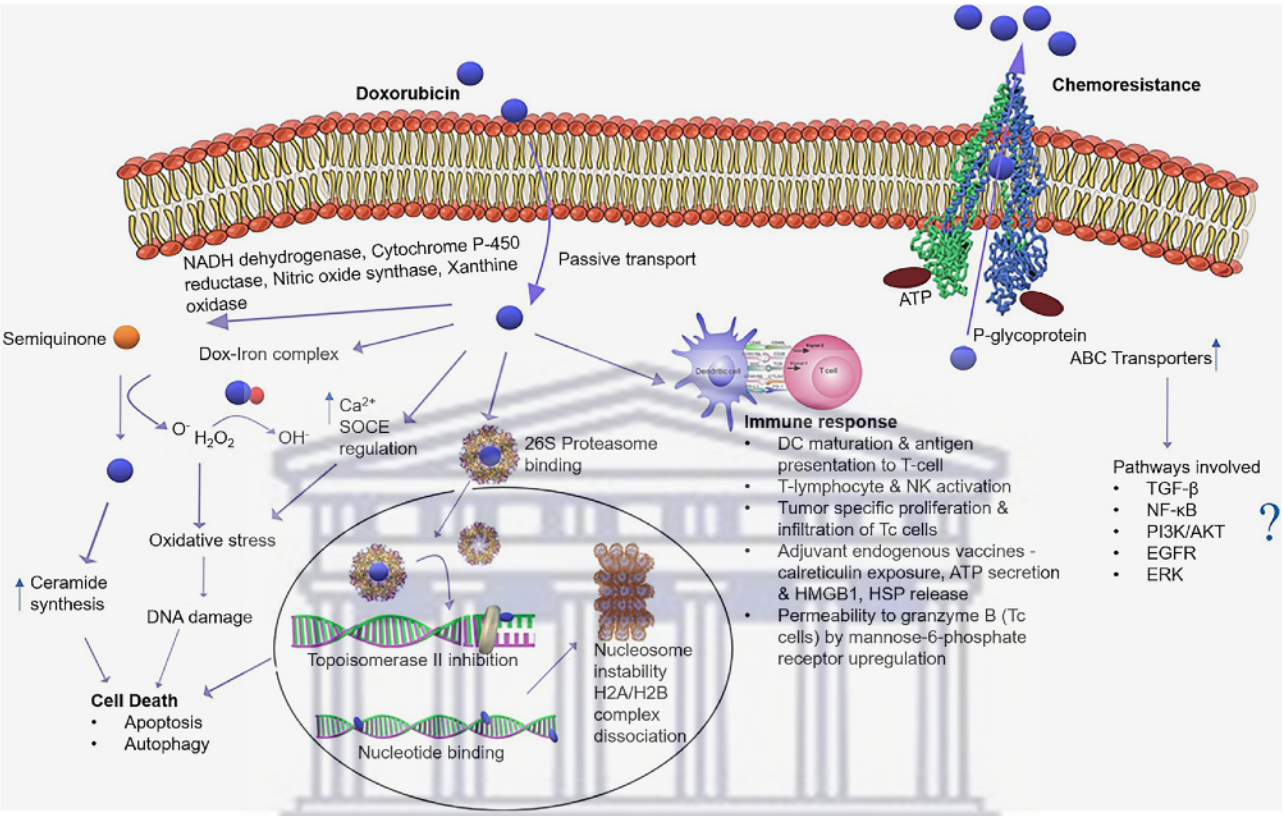

Figure 6: Overall molecular targets of doxorubicin, as well as the possible pathways involved in the development of chemoresistance (Sritharan and Sivalingam, 2021).

1.3.3.1 Doxorubicin Administration

Doxorubicin is routinely administered intravenously and intravesically, and must not be administered orally, subcutaneously, intramuscularly, or intrathecally. Doxorubicin injections should only be administered by qualified physicians with extensive experience in cytotoxic therapy. When administered intravenously, the solution is given via the tubing of a free flowing infusion of sodium chloride or dextrose within 2-15 minutes. This technique minimises the risk of thrombophlebitis or perivenous extravasation, which can ultimately lead to severe local cellulitis, vesication and tissue necrosis. Furthermore, a direct intravenous injection is not recommend due to the risk of extravasation, which may occur even if adequate blood flow returns upon needle aspiration. The dosage of doxorubicin administered depends on the dosage regimen, the general health status of the patient, and the previous treatment history of the patient (Accord Healthcare, 2022).

1.3.3.2 Doxorubicin Side Effects

Doxorubicin chemotherapy may result in the undesired toxicity of cardiomyocytes, cardiac fibroblasts, cardiac progenitor cells, endothelial progenitor cells, smooth muscle cells, and mesenchymal stem cells (Sritharan and Sivalingam, 2021). Cardiotoxicity associated with conventional doxorubicin therapy can be classified as either acute or chronic (Rivankar, 2014). Early effects seen following a single dose of doxorubicin are left ventricular dysfunction in patients with borderline cardiac compensation and arrhythmias. The later effects observed are dose-dependent cardiomyopathy, of which some may result in congestive heart failure (Von Hoff, 1979). The main mechanism of cardiotoxcity is hypothesised to occur via iron oxidation and the generation of free radicals. Furthermore, doxorubicin has been reported to disrupt cardiac iron hemostasis through its interaction with iron regulatory proteins (IRE 1 and 2) and ferritin. Doxorubicin in addition to its metabolite, doxorubicinol, has also been known to induce cardiac dysfunction via its binding and its altering of the functionality of Ca^{2+} ATPase of sarco/endoplasmic reticulum (SERCA2A), and the reduction of thiol groups of ryanodine receptor (RyR2) (Sritharan and Sivalingam, 2021). Additional side effects associated with the use of doxorubicin are described in Table 5.

Table 5: Additional doxorubicin side effects, grouped by frequent, less frequent and rare.

Frequent Side Effects	Less Frequent Side Effects	Rare Side Effects
Alopecia	Chronic heart failure	Allergic dermatitis
Esophagitis	Diarrhea	Allergic reactions (Anaphylaxis)
Infection at injection site	Gastrointestinal ulcers	Bronchospastic pulmonary disease
Leukopenia	Gout	Cardiotoxicity
Nausea	Hyperuricemia	Drug fever
Stomatitis	Injection site sequelae	Dyspnea
Urine and tear discoloration	Nail discolouration	Extravasation injury
Vomiting	Phlebosclerosis	Myelodysplastic injury
	Postirradiation erythema	Pruritus of skin
	Skin thickening	Severe bone marrow depression
	Thrombocytopenic disorder	Skin rash
	Tissue necrosis	Urticaria
	Uric acid nephropathy	Wheezing

1.4 Nanotechnology

The ideas and concepts behind nanoscience and nanotechnology began in 1959 when physicist Richard Feynman gave a talk entitled "There's Plenty of Room at the Bottom". In his talk, Feynman described a process in which scientists would be able to manipulate and control individual atoms and molecules. Approximately a decade on from that ground-breaking talk, Professor Norio Taniguchi coined the term "nanotechnology" with his work on ultraprecision machining (National Nanotechnology Initiative, 2022). Ultimately, nanotechnology is the use of materials on the nanoscale. There are various benefits involved when working at such a small scale, for example, treatment and target sites are very specific consequently leading to more precise and efficient therapies (British Society for Nanomedicine, 2012). In the field of nanomedicine, these technologies are applied in the healthcare system to improve current imaging and diagnostic techniques as well as therapeutics (Joo, Visintin and Mor, 2013). An example of this is the use of nanoparticles to improve the efficacy and effectiveness of drugs. Some drugs may not be as effective because they have a low solubility in water, and therefore the human body may not be able to absorb enough of the drug. Additionally, certain drugs have severe side effects and this may be due to poor delivery of the drug to actual sites of disease. Nanomedicines, therefore, play an important role in making sure enough of the drug enters the body, stays in the body long enough, and also ensures the drugs are delivered to the correct sites for treatment (British Society for Nanomedicine, 2012).

The importance of nanotechnology is now apparent to all scientists and even governmental entities worldwide. To this extent, in 2016 Gao et al. reported that more than 60 countries have launched their own national nanotechnology programs. Furthermore, there is an increasing interest in developing educational programs related to nanotechnology for all levels of education (Kargozar and Mozafari, 2018). South Africa itself has "The National Nanotechnology Strategy" developed by the South African Nanotechnology Initiative (SANi). This strategy has been widely promoted because of the future prospects of this field. There is an increased interest in nanoscience globally, and in order for South Africa to remain competitive at a global scale, and to alleviate problems such as unemployment, poverty, underdevelopment, and many other issues, it is crucial to develop science and technology in the country. Whilst the South African industry and researchers have been involved in nanoscience and nanotechnology for a considerable amount of time, new generations of this technology are emerging rapidly and in order for the country to remain in touching distance

with first-world countries, development in this field of expertise is crucial (National Nanotechnology Initiative, 2022).

1.4.1 Classification of Nanomaterials

Various classification systems have been constructed to organise nano-sized materials. In general nanomaterials are classified based on their dimension and composition. Based on their dimensions, naomaterials can be classified as zero dimension, one dimension, two dimension, and three dimension (Kargozar and Mozafari, 2018). However, ultimately nanomaterials can be broadly classified into four categories, namely, carbon nanomaterials, metal and metal oxide nanomaterials, organic nanomaterials, and nanocomposites (Khan, 2020).

1.4.1.1 Carbon Nanomaterials

Fullerenes (Bucky-balls) and carbon nanotubes (CNTs) represent two of the major classes of carbon-based nanoparticles. Fullerenes contain nanomaterials that are constructed by globular hollow cage such as allotropic forms of carbon. They have generated huge amounts of interest in the commercial sector due to their good electrical conductivity, high strength, structure, electron affinity, and versatility. In addition these materials posses arranged pentagonal and hexagonal carbon units where each carbon is sp^2 hybridised. CNTs are elongated tubular structures, 1-2nm in diameter. These can be predicted as either metallic or semiconducting depending on their diameter. Structurally these resemble graphite sheets that roll upon themselves. The rolled sheets can be single, double or many-walled and are therefore named as single- walled (SWNT), double-walled (DWNT) or multi-walled carbon nanotubes (MWNT) respectively. Due to their unique physical, chemical and mechanical characteristics, these materials are not only used in pristine form but also in nanocomposites for many commercial applications such as fillers, gas adsorbents and as support mediums for many organic and inorganic catalysts. (Khan, Saeed and Khan, 2019).

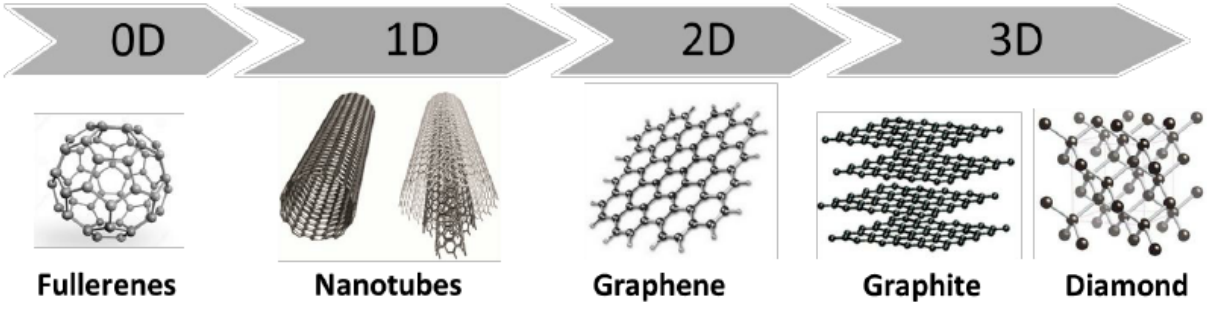

Figure 7: Types of carbon nanomaterials in addition to their dimensions.

1.4.1.2 Metal and Metal Oxide Nanomaterials

Metal and metal oxides can also be used to generate nanomaterials. Some of the most common metal and metal oxide nanomaterials are synthesised using gold, silver, titanium dioxide, and zinc oxide (Khan, 2020). Metal nanoparticles, such as gold and silver, are extensively used in cell imaging, DNA hybridisation detection, protein interactions, and photothermal therapy due to their extremely strong absorption and light scattering owing to their surface plasmon resonance (Khlebtsov and Dykman, 2010). Ultimately, the high attractiveness of using gold and silver nanoparticles is due to their unique optical properties, photothermal properties, facile surface chemistry, and their size (Ficai, Ficai and Andronescu, 2015). It has also been reported that both gold and silver nanoparticles are effective in inhibiting the growth of gram-positive and gram-negative bacteria, however this requires a lot more research.

1.4.1.3 Organic Nanomaterials

For the most part, organic nanomaterials contain organic matter, without carbon or inorganic-based materials. An interesting characteristic of organic nanomaterials is that they possess non-covalent bonds that are typically weak in nature meaning they are easily broken. This means organic nanomaterials can be easily modified to produce different shapes of nanomaterials such as liposomes, dendrimers, polymers and micelles (Khan, 2020).

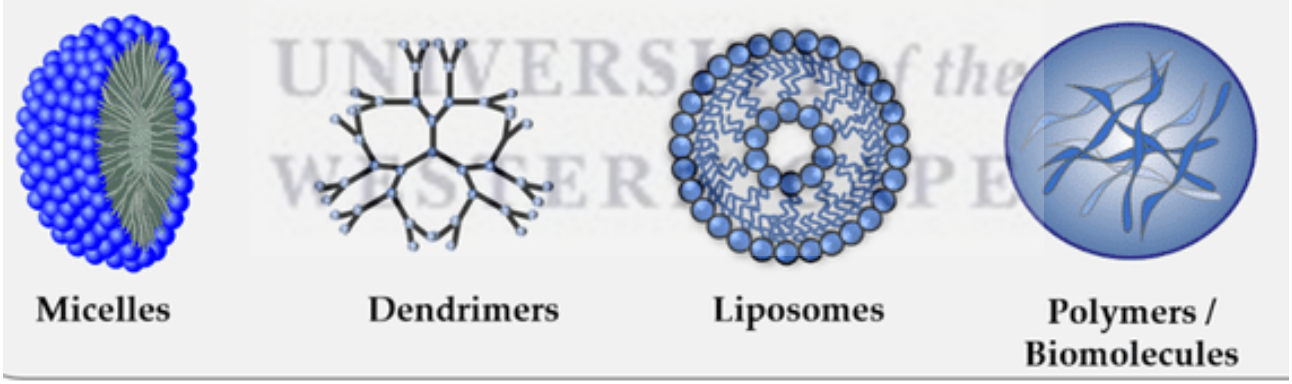

Figure 8: Types of organic nanomaterials.

1.4.1.4 Nanocomposites

A nanocomposite combines two or more materials, of which at least one is a nanomaterial, and with different chemical and physical properties. Nanocomposite materials are designed to display properties that exceed the capabilities of constituent parts. Nanocomposites are made by embedding

materials (the reinforcing phase) into another material (the matrix phase). Typically, reinforcing materials are strong with low densities, whilst the matrix is commonly flexible or tough material (Khan, 2020). Figure 9 below shows the structure of a typical nanocomposite.

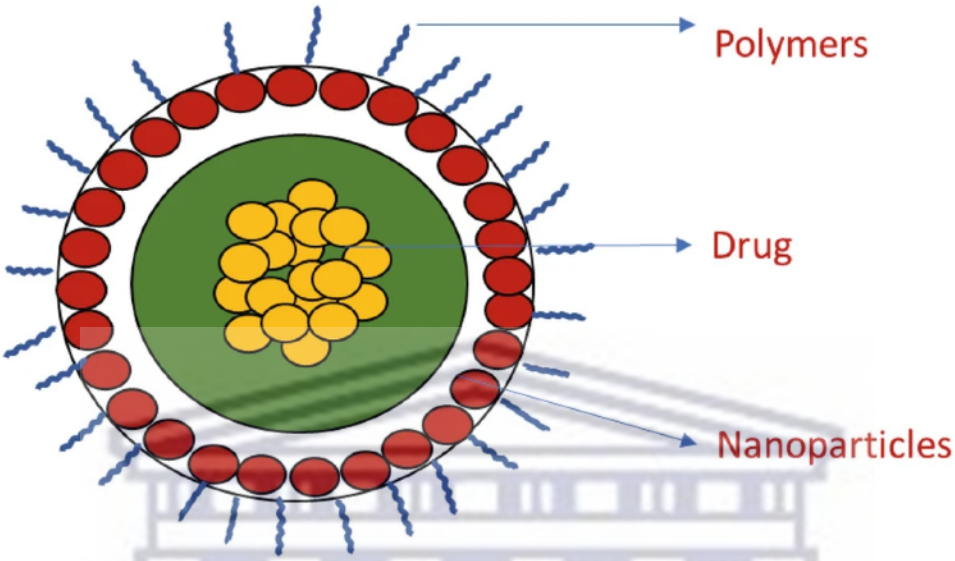

Figure 9: Typical structure of a nanocomposite (Khan, 2020).

1.4.1.5 Nanomaterial Origins

In addition to the classification categories mentioned above, nanomaterials can also be classified based on their source of origin. Generally, they can be classified as natural nanomaterials or synthetically produced nanomaterials. Natural nanomaterials can be generated in biological organisms such as microbes, plants, and also via anthropogenic actions (Khan, 2020). The creation of natural nanomaterials is easily accessible as they are present in the hydrosphere, atmosphere, lithosphere, and biosphere. Our planet itself is comprised of nanomaterials that are naturally formed and present in microbial organisms including humans (Hochella, Spencer and Jones, 2015). The most common method used to produce nanomaterials is the synthetic method, which uses biological, physical, chemical, or hybrid methodology. One of the greatest advantages of using synthetically produced nanomaterials is the possibility to produce large amounts with different shapes and sizes, whilst maintaining great precision and accuracy. However, a major concern associated with synthetic nanomaterials is whether there is sufficient knowledge to predict their performance. Furthermore, they display different environmental behaviour which is different from natural nanomaterials (Khan, 2020).

1.4.2 Nanoparticle Synthesis

Various methods can be used for the synthesis of nanoparticles, however these methods are broadly divided into two main categories (see Figure 10). These categories are the top-down and bottom-up approaches, which are further divided into various subclasses based on the operation, reaction condition, and adopted protocols (Khan, Saeed and Khan, 2019). Top-down synthesis employs destructive approaches starting from larger molecules which decompose into smaller molecules, and ultimately suitable nanomaterials. Examples of common top-down approaches include grinding/ milling and physical vapor deposition. Bottom-up synthesis is essentially the opposite of top-down synthesis. In these methods, nanomaterials are generated from relatively smaller substances into their desired structures. Examples of common bottom-up approaches include sedimentation and reduction techniques (Iravani, 2011).

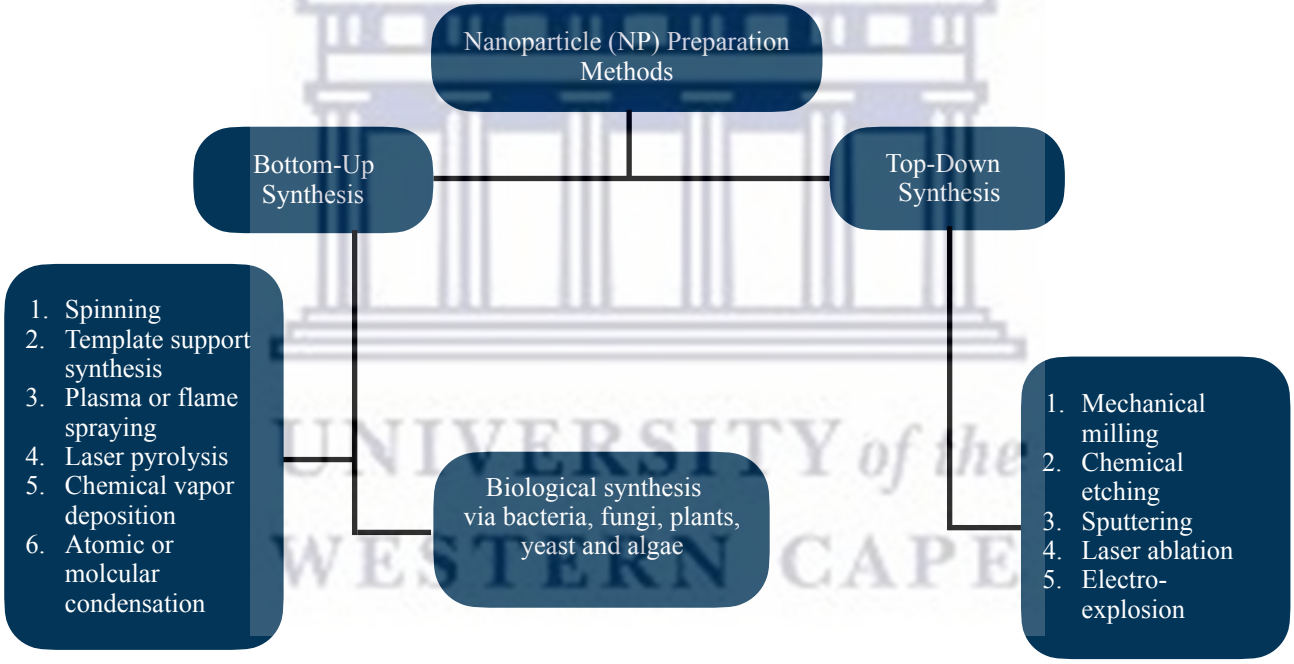

Figure 10: Schematic diagram illustrating typical synthesis methods for nanoparticles (Khan, Saeed and Khan, 2019).

1.5 Cancer Nanotechnology

Cancer nanotechnology is a field of interdisciplinary research that merges the fields of biology, chemistry, engineering, and medicine. This field is expected to lead major advances in cancer detection, diagnosis, and treatment. The fundamental theory is that metal, semiconductor and

polymeric particles have novel optical, electronic, magnetic, and structural properties that are often not observed in individual molecules or bulk solids (Nie, Xing, Kim and Simons, 2007). Besides their use as drug delivery systems, nanomedicines may also be used as synthetic scaffolds for imagining probes in the detection of cancers, and this is due to their unique physiochemical properties (Salvioni et al., 2019). Recently, advancements in nanomedicine research have led to the production of "smart" nanocarriers, some of which contain both drugs and imaging agents in a single system. Such nanotheranostics make it easier to monitor the biodistribution of drugs and provide flexibility when analysing target site accumulation. Additionally, they also allow the visualisation and quantification of drug release from nanomedicines (Alshehri et al., 2020).

The main complication with any cancer therapy is to acquire the desired concentration of therapeutic agent at the tumor site so that cancer cells are destroyed whilst minimising damage to healthy cells (Rizwanullah et al., 2020). As a matter of fact, research in the area of cancer nanotechnology is growing at a rapid rate, however its clinical translation and approval of cancer nanomedicines is quite slow. The most distinguished clinically approved nanomedicines used in the management of different cancers are Doxil®/Caelyx® and Abraxane®. Doxil® is a liposomal formulation of doxorubicin, which has been approved for the treatment of Kaposi's sarcoma, refractory breast cancer, and ovarian cancer. Abraxane® on the other hand, is an albumin-based nanoparticle of paclitaxel, which has been approved for the management of metastatic breast cancer. In the field of diagnostics, Resovist® and Feridex®/Endorem® which are iron oxide nanoparticles, have been approved for liver/spleen lesion imaging. Interestingly, the majority of the nanotherapeutic and diagnostic agents that have been approved are organic in nature, this may be due to their increased biocompatibility and negligible toxicity (Alshehri et al., 2020).

1.5.1 Liposomal Doxorubicin Carriers

Due to the side effects associated with the use of doxorubicin, research is being aimed at exploring safer delivery systems which maintain a high level of efficacy. Several systemically administered liposomal doxorubicin formulations have been investigated and approved, including pegylated (Doxil® and Lipodox®) and unpegylated (Myocet®) forms. In all formulations, the liposomes incorporate doxorubicin into an aqueous core (Gupta and Ngan, 2016). It is important to note that a better safety profile is observed with liposomal doxorubicin formulations compared to conventional doxorubicin as patients treated with liposomal formulations exhibit less cardiotoxicity, nausea, vomiting, and less myelosuppression (Chatterjee, Zhang, Honbo and Karliner, 2010). This is likely

due to the increased accumulation of liposomal doxorubicin in tumor tissue, with decreased concentrations in healthier tissues, via an enhanced retention and permeability effect (EPR). Based on increased leakiness of tumor blood vessels and reduced lymphatics, EPR permits passive targeting of liposomes to tumor cells compared to surrounding tissues. Nanoparticles between 10-200nm are dependent on EPR for their build-up in tumors (Zhao, Woodle and Mixson, 2018).

1.5.2 Micelle Doxorubicin Carriers

Polyionic complex micelles have been developed to co-deliver plasmids and doxorubicin to tumor cells *in vitro*. In the study, A blocked polymer of Tat peptide (TAT), polyethylene glycol (PEG), and polyethylenimine (PEI) was complexed with plasmid DNA to form the complex micelle, whereafter doxorubicin was conjugated to PEI via a pH-sensitive hydrazine bond. The cytotoxicity and dose-response of the conjugate was compared to free doxorubicin, where free doxorubicin had a more toxic effect than the conjugate. It was speculated that this may be due to the delayed release of doxorubicin from the micelle complex (Liu et al., 2013).

Additionally, studies combining both curcumin and doxorubicin within a micelle nanoparticle have demonstrated greater antitumor activity than their separate counterparts. The micelles were composed of a PEG doxorubicin conjugate (PEG-Dox) formed via a pH-sensitive Schiff's base. Additionally, curcumin was incorporated within the micelle via a hydrophobic interaction with the PEG-Dox conjugate, to form the nanoparticle-doxorubicin-curcumin complex (NP-Dox-Curcumin). Ultimately this formed spherical nanoparticles that were approximately 180nm in size. The study ultimately concluded that the NP-Dox-Curcumin complex inhibited tumor growth by nearly 70% compared to untreated groups, whereas doxorubicin and curcumin mixtures as well as the PEG-Dox conjugate only inhibited tumor growth by 40% (Zhang et al., 2016).

1.5.3 Alternative Doxorubicin Carriers

Recently, exosomes have also been used to deliver doxorubicin. Exosomes are a subclass of extracellular vesicles with sizes between approximately 30-200nm. In 2016, Hadla et al. demonstrated that doxorubicin-loaded exosomes administered via IV transfusion twice weekly completely inhibited the growth of MDA-MB-231 tumor xenografts. Interestingly, the efficacy of these exosomes was similar to Doxil®. Furthermore, in a syngeneic model of ovarian cancer, the exosomes inhibited tumor growth significantly more compared to the maximum tolerated dose of free doxorubicin whilst significantly decreasing the risk of cardiotoxicity (Hadla et al., 2016). In

other studies, doxorubicin has been conjugated to magnetic carriers, where the drug is directed to tumors with an external magnet. Wuang et al. demonstrated that a combination of lower pH and nanoparticle preheating to 42°C increases doxorubicin release from these nanoparticles leading to an enhanced cell killing (Wuang et al., 2011).

1.5.4 Polymeric Doxorubicin Carriers

In 2006, Lee et al. demonstrated that a single dose of a dendrimer-Dox conjugate cured mice with subcutaneously implanted colon cancer, which is significant considering C-26 colon carcinoma cells are resistant to doxorubicin. Their 8nm carrier was composed of a polyester dendrimer-PEG conjugate with a topologically globular structure. Due to the structure of the conjugate, the covalently bound doxorubicin was thought to be located within the interior of the nanoparticle. At the maximally tolerated dose of the conjugate, 100% of the tested mice subjects survived compared to only 90% treated with Doxil®. Additionally, the authors noted the potential advantage of using a dendrimer conjugate compared to Doxil®, as a variety of drugs could be attached (Zhao, Woodle and Mixson, 2018).

A similar effort targeted liver cancer with doxorubicin-loaded polymeric nanoparticles. The nanoparticles were furnished with pullalan (Pul) and/or arabipogalactan (AGn), of which both target asialoglycoprotein receptors. *In vitro* studies demonstrated that the ligand-targeting nanoparticles have increased uptake into HepG2 cells (liver cancer cells) compared to non-targeting nanoparticles. Their study concluded that the Pul-NP-Dox conjugate showed the greatest inhibition of HepG2 cells that had been implanted subcutaneously with a 75% reduction compared to the untreated group. Furthermore, they demonstrated that mice treated with the Pul-NP-Dox conjugate showed little to no cardiotoxicity, whereas mice treated with conventional doxorubicin demonstrated significant cardio and renal toxicity (Pranatharthiharan et al., 2017).

1.5.4.1 Chitosan

Chitosan (CS) is a linear polysaccharide composed of glucosamine and N-acetylglucosamine units. It is biocompatible, biodegradable, and non-toxic in oral drug delivery systems. The addition of CS does not only give the nanoparticles a positive surface charge, but it also prolongs the the time in which active compounds are in contact with the epithelium, which consequently enhances absorption via paracellular transport pathways through tight junctions (Dai et al., 2008). This bioactive polymer has been used to synthesise nanoparticles that deliver chemotherapy agents and

nucleic acids. In an early study conducted in 2001, Mitra et al. incorporated a dextran-doxorubicin conjugate into a CS-NP. They compared the tumor-reducing ability and survival-prolonging ability of conventional doxorubicin, the dextran conjugate alone, and the dextran CS-NP. Their results demonstrated that mice treated with dextran CS-NPs showed the most effective tumor regression (50%) and the best survival rate (50%) at day 90, whereas all mice treated with conventional doxorubicin had died by day 60, and 25% of the mice treated with the dextran conjugate alone had survived by day 90 (Mitra, Gaur, Ghosh and Maitra, 2001). Similarly, in 2018 Verma et al. demonstrated that doxorubicin-loaded CS-NPs distinctly inhibited tumor growth and prolonged mice survival compared to conventional doxorubicin (Verma et al., 2018). Interestingly, both studies showed little to no evidence of toxicity in mice that received nanoparticle treatment.

1.5.4.2 Chitosan-Alginate Nanoparticles as Potential Carriers for Doxorubicin

Alginate (ALG) is a water-soluble linear polysaccharide extracted from brown sea weed and consists of interchanging blocks of 1-4 linked α-L-guluronic and β-D-mannuronic acid residues. Literature states that ALG is known to be mucoadhesive, biodegradable, and biocompatible and has the potential for numerous pharmaceutical and biomedical applications such as drug delivery systems and cell encapsulation (Dai et al., 2008). ALG nanoparticles and microparticles can be synthesised relatively easily by inducing gelation with calcium ions (Pan et al., 2002; Mladenovska et al., 2007). This relatively easy process produces a pre-gel consisting of very small aggregates of gel particles. Following this, an aqueous polycationic solution is added to produce a polyelectrolyte complex coating. Poly-L-lysine (PLL), a natural cationic polymer, has been previously used in combination with ALG to prepare these types of nanoparticles. However, due to its toxicity and immunogenicity when injected, chitosan (CS) has been selected as an alternative (Dai et al., 2008). The addition of CS stabilises the core into distinct sponge-like nanoparticles consisting of a core-shell structure.

A study by Katuwavila et al., (2016) demonstrated the promising potential of using a chitosan-alginate nanoparticle delivery system to encapsulate doxorubicin. The nanoparticles were prepared using a novel ionic gelation method that used alginate as the cross-linker. The alginate and doxorubicin form the core of the nanoparticle which is then “encapsulated” by chitosan. By incorporating alginate into the system, the nanoparticles were more stable, had a higher positive zeta potential, and had a higher encapsulation efficiency compared to chitosan cross-linked with sodium tripolyphosphate. *In vitro* cytotoxicity assays also showed a notable difference in the effect

of a nanoparticle system compared to free doxorubicin. Additionally, assays demonstrated that free doxorubicin shows dose-dependent cytotoxicity, whilst doxorubicin delivered by the nanoparticle systems showed both a dose, and time-dependent cytotoxicity (Katuwavila et al., 2016).

Magnetic alginate-chitosan nanoparticles have also been used in the targeted therapy of human breast cancer cells. A study by Song et al., (2018) synthesised magnetic alginate-chitosan nanoparticles in a layer-by-layer fashion which allowed for the encapsulation of curcumin. This system was designed to enhance the bioavailability, uptake efficiency, and cytotoxicity of curcumin in human breast cancer cells. 3-(4,5-Dimethylthiazol-2-yl)-2,5-Diphenyltetrazolium Bromide (MTT) assays showed that the nanoparticle system significantly increased cytotoxicity and encapsulation efficiency. Thus, they concluded that magnetic alginate-chitosan nanoparticles provide promising candidates for cancer therapy (Song et al., 2018).

The literature, therefore, supports the notion that efficient target therapies are essential in the battle against cancer. These therapies can be developed using novel nanotechnology approaches and can ultimately decrease the side effects caused by treatments such as conventional chemotherapy, which are toxic to the body and essentially harm healthy cells.

Introduction

1.6 Problem Statement and Purpose of Study

1.6.1 Problem Statement

Among all childhood cancers diagnosed, neuroblastoma is the most prevalent during infancy. Neuroblastoma continues to perplex scientists and oncologists alike because its biological and clinical behaviour fluctuate between complete spontaneous regression and clinical multidrug resistance, strongly indicating that besides genetic events, the tumor microenvironment significantly influences these characteristics of neuroblastoma (Borriello et al., 2019; Mullassery and Losty, 2016). Although the development of novel antitumor agents such as isotretinoin, ^{131}I-MIBG, irinotecan, and dinutuximab has increased survival rates among neuroblastoma patients, those suffering from high-risk disease still remain a challenge. Furthermore, treatment for patients with high-risk neuroblastoma involves aggressive strategies, leading to both short and long-term toxicity (Rodríguez-Nogales, Noguera, Couvreur and Blanco-Prieto, 2019).

Nanotechnology provides some promising answers to this challenge, as drug delivery systems have shown numerous benefits such as improving drug bioavailability and biodistribution (Ravi Kumar, Blanco-Prieto and Waterhouse, 2013). Nanomedicines include several colloid systems at the nanoscale (1-1000nm), and can be composed of various materials such as polymers, lipids, and metals that are able to encapsulate multiple therapeutic agents. One of the reasons thought to be behind the success of nanotherapeutics is their EPR effect in tumor tissues. Additionally, nanocarriers can be functionalised at their surface with specific target moieties so they can deliver therapeutic agents directly to tumor tissues, or with molecules such as PEG to increase their circulation in the blood (Rodríguez-Nogales, Noguera, Couvreur and Blanco-Prieto, 2019). Finally, nanotechnology has also demonstrated promising results in the field of cancer detection due to the unique physicochemical properties of NPs (Chen et al., 2018).

1.6.2 Purpose of Study

It is well documented that whilst treatment with conventional doxorubicin is relatively effective, the short and long-term side effects associated with its use is a great challenge. Since neuroblastoma rarely occurs in adults and children over the age of 10, finding a safe and efficient therapy can help decrease the mortality rate of children who suffer from these malignancies. These treatments can

lead to a better quality of life for children who often suffer from severe side effects as a result of conventional treatments such as radiation and chemotherapy. This study will focus on the synthesis of a chitosan-alginate (CS-ALG) nanoparticle that will be used to encapsulate doxorubicin. The resulting NPs will be analysed to evaluate their characteristics as well as their potential cytotoxic effects on the SK-N-BE(2) neuroblastoma cell line. Additionally, the possible mechanism of action of the NPs may be studied. The results of this study could possibly lead to the development of a novel, more efficient delivery mechanism for doxorubicin in neuroblastoma therapy.

1.6.3 Aim and Objectives

The aim of the study is to investigate the effect and possible mechanism of action of doxorubicin-loaded chitosan-alginate nanoparticles on SK-N-BE(2) neuroblastoma cells in comparison to free doxorubicin.

The objectives of the following study are:

1. To synthesise and characterise doxorubicin-loaded chitosan-alginate nanoparticles (DX-CS-ALG), and chitosan-alginate nanoparticles (CS-ALG)
2. To examine whether DX-CS-ALG and CS-ALG have an antagonistic effect on SK-N-BE(2) neuroblastoma cells.
3. To obtain the IC-50 of DX-CS-ALG
4. To examine the optimal concentration of DX-CS-ALG in inhibiting cell proliferation
5. To examine the effect of DX-CS-ALG on SK-N-BE(2) cellular morphology
6. To observe the possible mechanism of action of DX-CS-ALG

1.6.4 Hypothesis

The DX-CS-ALG nanoparticle system will have a greater antagonistic effect than free doxorubicin on SK-N-BE(2) cell proliferation and morphology.

1.6.5 Null Hypothesis

The DX-CS-ALG nanoparticle system will not have a greater antagonistic effect on SK-N-BE(2) cell proliferation and morphology compared to free doxorubicin.

Chapter 2
Methodology

2.1 Experimental Design

The main focus of this chapter is to outline and describe the design of the experiment, including the nanoparticle synthesis and characterisation, as well as the research methodology carried out for the study. This chapter will summarise the materials and methods used, such as the chemicals required, the drugs tested, the assays carried out, and the maintenance of the SK-N-BE(2) neuroblastoma cell line. Normal growth of the SK-N-BE(2) cells was analysed by the means of the Trypan blue assay. Cell viability and cytotoxicity were analysed utilising the MTT tetrazolium assay, and the graphs and dose-response curves were constructed on GraphPad Prism (GraphPad Prism version 8 for Mac, GraphPad Software, San Diego California USA, www.graphpad.com). Additional assays such as the Reactive Oxygen Species (ROS) assay were carried out to determine the nanoparticles ability to induce oxidative stress.

2.2 Drugs and Chemicals

The drug used in this study was Doxorubicin (D1515-10MG, CAS 25316-40-9) (Sigma-Aldrich, St Louis, MO, USA). Chemicals used for nanoparticle synthesis included glacial acetic acid (A6283-500ML, Product Code: 1003219805) (Sigma-Aldrich, St Louis, MO, USA), alginic acid sodium salt (180947-250G, Product Code: 1002939832) (Sigma-Aldrich, St Louis, MO, USA), and low molecular weight chitosan (448869-50G, Product Code: 102344491) (Sigma-Aldrich, St Louis, MO, USA). Chemicals used outside synthesis included heat-inactivated foetal bovine serum (FBS) (Gibco, Paisely, UK), phosphate-buffered saline (PBS) (Gibco, Paisely, UK), 1X Trypsin-Versene (EDTA) (Lonza, WhiteSci, Walkersville, USA), Dulbecco's Modified Eagles Medium supplemented with F-12 glutamax (DMEM-F12 glutamax) (Gibco, Paisely, UK), penicillin/ streptomycin (Pen-Strep) (Lonza, WhiteSci, Walkersville, USA), dimethyl sulfoxide (DMSO) (472301-2.5L, Product Code: 1003192726) (Sigma-Aldrich, St Louis, MO, USA), 0.4% trypan blue (Lonza, WhiteSci, Walkersville, USA) and thiazolyl blue tetrazolium bromide (MTT) reagent (Sigma-Aldrich, St Louis, MO, USA). All plastics used for cell culture and assays were obtained from SPL Life Sciences (purchased through Bio-Smart Scientific).

2.3 Maintenance of SK-N-BE(2) Cell Line

Cells used for this study were gifted to our lab by a fellow colleague in the Department of Medical Bioscience at The University of The Western Cape. Cellular morphology of the SK-N-BE(2) cells varies, with some cells having long processes and others that are epitheloid-like. When cultured, these cells tend to aggregate, form clumps and float (LGC Standards, 2022). Dulbecco Modified Eagle's Medium (DMEM-F12) supplemented with 10% heat-inactivated FBS and 1% of 0.5 mg/ml Pen-Strep was used to maintain the SK-N-BE(2) cells in a 5% CO_2 and 95% O_2 atmospheric condition at a temperature of 37°C. The cells used in the experiments were from passages 12 to 25. Cells were cultured in a NuAire DHD NU-5510E autoflow automatic CO_2 air-jacketed incubator and an AireGard NU-201-430E horizontal laminar airflow cabinet with a HEPA-filtered clean work area (NuAire) in the Molecular Oncology lab at The University of The Western Cape.

2.4 Sub-Culturing and Cell Stock Storage

The SK-N-BE(2) cells were grown on cell culture petri dishes until they had reached confluency. Once confluency had been reached, cells were split and subcultured or seeded for experiments. First, growth media was aspirated and the cells were washed with PBS to remove any waste products. Thereafter, 1X Trypsin-EDTA was added, and the culture flasks were incubated for approximately 3-5 minutes to detach the cell monolayer from the dish. Following incubation, the dish was transferred back into the laminar flow where an equal or greater amount of complete growth media was added to neutralise the effects of the trypsin added. The detached cells were then aspirated and added to a 15ml conical tube. Hereafter, the appropriate number of cells were added to new culture flasks containing fresh complete growth media.

Cell stocks were stored in cryovials containing 1 ml of cryopreservation media (DMEM supplemented with 10 % FBS and 5% DMSO) at -80°C. These stocks were produced by trypsinizing cells and centrifuging the subsequent suspension at $1x25G$ for 10 minutes to form a pellet at the bottom of the tube. Hereafter, the supernatant was removed and the pellet was resuspended in cryopreservation media. Subsequently, the resuspension was transferred to cryovials kept on ice which are stored at -80°C as stocks for future use.

2.5 Growth Curve Analysis

A variety of assay methods are used to estimate the number of viable cells in a population, but the Trypan Blue assay is most frequently used. Trypan Blue is a dye that is excluded from live cells but taken up or accumulates in dead cells. Thus, the Trypan Blue assay assists in accurately assessing the viability of cells in a given population. (Strober, 2015).

SK-N-BE(2) cells were trypsinized from culture flasks after they had reached confluency and transferred to a 15 ml conical tube. A cell count was carried out to count the number of cells in solution to carry out the density seeding calculation. Cells were seeded into a 24-well plate at a density of $1x10^5$ cells per ml. Following seeding, the plate was incubated for 24, 48 and 72 hours. After each incubation period, the cells were harvested with Trypsin and counted using the Trypan Blue assay. For each time point the experiment was carried out 8 times and the results were averaged. The plate layout below in Figure 11 shows how the cells were seeded for each time point.

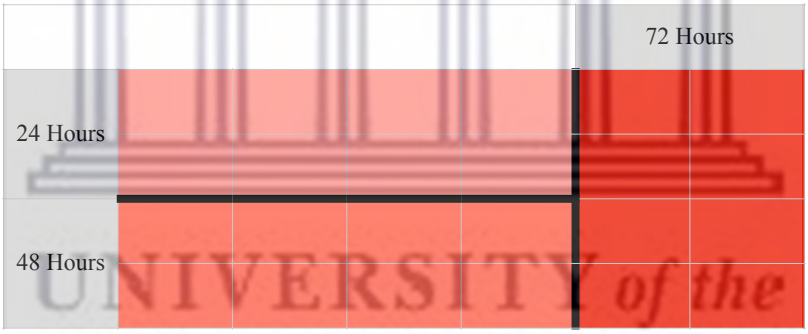

Figure 11: Growth curve plate layout showing the wells used for each time point (untreated).

2.6 Synthesis by Ionotropic Gelation

Several methods and materials are implemented when synthesising nano- or microparticles for biomedical applications, from carbon-derived structures to metallic and lipid particles. However, the most desirable method for synthesising polymeric nanoparticles is ionotropic gelation (IG). This method is one of the more affordable and easier procedures to carry out for daily lab work. IG for nano-encapsulation of proteins was first described by Calvo et al., in 1997. The authors presented a detailed study on the synthesis of CS nanoparticles in the presence of sodium tripolyphosphate (TPP). Their particular reaction took advantage of the cationic nature of CS in the presence of

diluted acids and the polyanioinic nature of TPP. Based on this work, Wu et al., used this system to successfully encapsulate anti-cancer drugs, whilst several other authors have encapsulated drugs such as insulin (Pedroso-Santana and Fleitas-Salazar, 2020). The intended method for this project will be adapted from Katuwavila et al., (2016). Electrostatic interactions between CS and ALG lead to the formation of CS-ALG beads, that have a CS core and a CS-ALG surface. Some researchers report that by adding a salt to the classic IG procedure, the stability of the interaction can be increased. For this purpose, salts such as calcium and zinc have been used. Consequently, this leads to the pre-gelation phase between one of the polymers and a salt, followed by the polyelectrolyte complexation phase in which the second polymer is added (Pedroso-Santana and Fleitas-Salazar, 2020). In 2011 Patil, Marapur, Kamalapur and Shiralshetti reported that this two-phase IG method leads to the generation of more stable CS-ALG particles.

2.6.1 DX-CS-ALG Nanoparticle Synthesis

In the present study, CS and ALG stock solutions were prepared at concentrations of 0.2% (m/v) and 0.1% (m/v) respectively. It is important to note that CS was dissolved in 1% acetic acid (AA), whilst ALG was dissolved in distilled water (dH_2O). Following optimisation, i.e. determining the best working concentrations of CS and ALG from the stock solutions to obtain the smallest NPs possible with ideal characteristics, working concentrations of 0.06% and 0.02% were selected for CS and ALG respectively. Following preparation of the working solutions, their pH was adjusted to 4.6 and 4.9 for CS and ALG respectively. To make solutions more acidic, hydrochloric acid was added drop wise whilst checking the pH between drops. To make a solution more basic, sodium hydroxide was added in a similar manner. Following pH adjustments, the CS solution was added drop wise to the ALG solution on ice (2:1 v/v ratio) under 50% probe sonication. During the encapsulation experiments, the desired concentrations of doxorubicin were added drop wise to the ALG solution first (1:1 v/v ratio) to form the pre-core solution. This was then followed by the addition of the CS solution in a similar manner to the unencapsulated experiments. Each set of experiments was carried out at least 4 times to ensure accuracy.

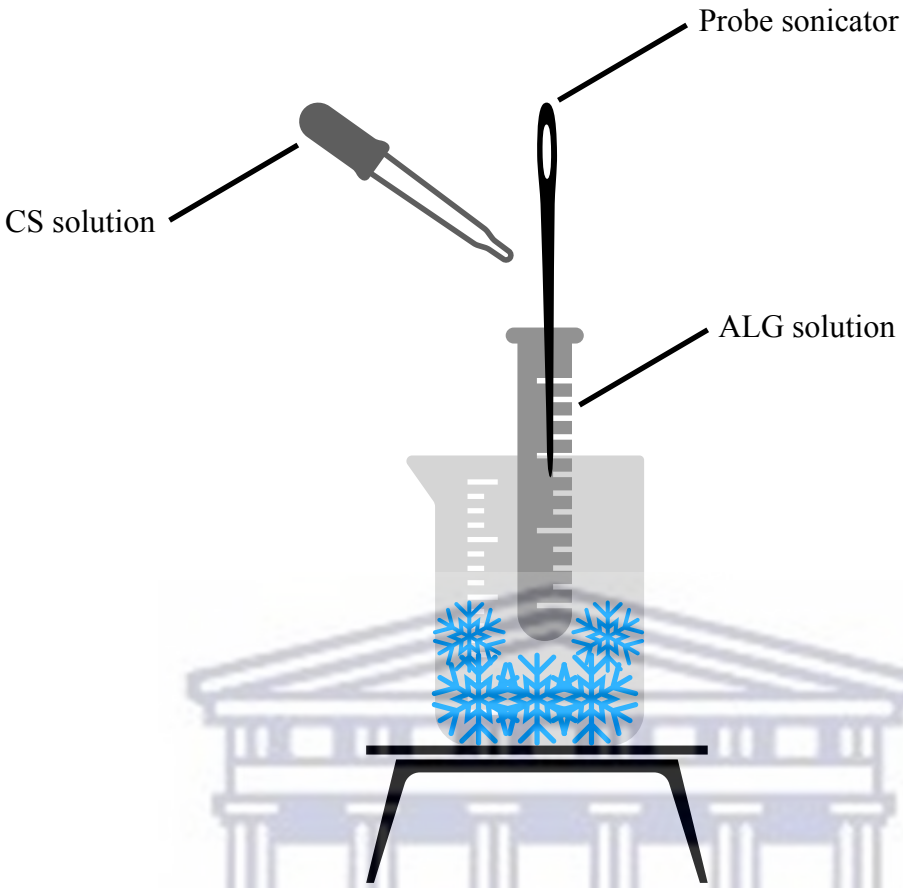

Figure 12: Schematic illustration of CS-ALG nanoparticle synthesis. In drug encapsulation experiments, the doxorubicin is added before the CS.

2.6.2 Nanoparticle Recovery and Characterisation

Following synthesis, the solutions were stored at 4°C overnight to ensure efficient drug encapsulation. Subsequently, the nanoparticles were recovered by centrifugation at 17 568 rcf for 45 minutes. This separated the nanoparticles into a clear gel-like pellet and a supernatant. The supernatant was then discarded and the pellet resuspended (washed) in dH_2O. Once the nanoparticles were resuspended, they were characterised using Dynamic Light Scattering (DLS). DLS is a technique usually used to find the size of nanoparticles in dispersion. The hydrodynamic diameter and polydispersity index (PDI) of the nanoparticles can also be determined by this technique. DLS approximates the size according to light scattered by particles under Brownian motion. When trying to optimise drug delivery using nanoparticles, the size of the system can affect its interaction with tissues or cell structures which can ultimately influence its pharmacokinetics and clearance (Pedroso-Santana and Fleitas-Salazar, 2020). Studying the zeta potential of the nanoparticles determines their stability, and this depends on their electrophoretic movement in

solution (Kumar et al., 2015). To determine the number of particles per ml, the washed solutions were freeze-dried and the resulting powder was weighed.

2.6.3 Transmission Electron Microscopy

Transmission electron microscopy (TEM) is the ideal instrument for the chemical and structural characterisation of nanoscale structures. Imaging, diffraction patterns and microanalytical information is easily produced and then integrated to give a comprehensive insight into the properties and behaviour of analysed nanomaterials (Smith, 2015). Chemical fixation is the first step in most protocols when preparing cells and tissues for TEM analysis. It is a vital step, as the quality of fixation affects the results obtained. The main purposes of chemical fixation is to stop metabolic processes, preserve the cellular fine structure, and stabilise the cells for subsequent steps in the preparatory procedure.

For the present, carbon coated copper grids were rendered hydrophilic using an EMS100 Glow Discharge Unit. Droplets of the sample were then diluted with water and neatly placed on the grids and were allowed to dry, or were negatively stained with 2% uranyl acetate. Once the grids were dry, they were imaged using the FEI T20 transmission electron microscope fitted with a LaB_6 emitter operating at 200kV. Finally, the images were collected using the Gatan US 1000 OCD camera (2048 x 2048 pixels).

2.6.4 Determination of Encapsulation Efficiency

The amount of incorporated doxorubicin will be determined by measuring the fluorescent absorbance of free doxorubicin remaining in the supernatant following centrifugation. Once a calibration curve is obtained, the percentage encapsulation efficiency can be calculated using equation 1 as shown below.

$$\% \text{ EE} = \frac{\text{Total DOX} - \text{Free DOX}}{\text{Total DOX}} \times 100.$$

Equation 1: Encapsulation efficiency for doxorubicin

2.7 Preparation of Doxorubicin Stock Solutions

All the reagents used were brought to room temperature and all plastics used were sterile.

A 100 mM stock solution of Doxorubicin was prepared by dissolving 6.6 mg of the powder (579.98 MW) in 110µl of DMSO. This was then further diluted to a 1mM (1000µM) working stock solution, which was then used to prepare the experimental stock solutions of log_2 concentrations: 0.015625µM - 16µM. These concentrations were made in complete growth media and stored in conical tubes and frozen at -20°C until treatment.

2.8 MTT Tetrazolium Reduction Assay

MTT tetrazolium reduction assay is a colorimetric assay that measures the reduction of yellow 3-(4,5-dimethythiazol-2-yl)-2,5-diphenyl tetrazolium bromide (MTT) by an enzyme in the mitochondria of living cells. Once in the mitochondria, it is reduced to an insoluble, purple, formazan product which is solubilised with an organic solvent such as isopropanol or DMSO. The formazan is measured spectrophotometrically at a wavelength of 560 nm (Groups.molbiosci.northwestern.edu, 2019). The inability of formazan to diffuse out of the cell membrane allows for its accumulation in living and healthy cells. This allows for the use of colour intensity as a determination of the number of viable cells in cell proliferation and cytotoxicity assays. The amount of formazan dye generated by the activity of the enzymes in the cells is directly proportional to the number of living cells.

2.8.1 Thiazolyl Blue Tetrazolium Bromide (MTT) Reagent Preparation and Protocol

MTT solution was prepared by adding 1 ml of sterile PBS to 5mg of 12mM Thiazolyl Blue Tetrazolium Bromide reagent. Following the addition of the MTT to the PBS, the solution was vortexed until the salt was completely dissolved. All MTT assays were carried out in 96 well flat bottom tissue culture plates.

2.8.2 Free Doxorubicin Experiment

For both the free drug experiments, and the drug encapsulated nanoparticle experiments, two time points were chosen; 24 and 48 hours. For the 24 and 48-hour assays, cells were seeded at densities of $5x10^4$ and $3x10^4$ cells per ml respectively. Following seeding, the SK-N-BE(2) cells were allowed

to attach for 24 hours under normal growth conditions. Once attached, growth media was aspirated from each well and the appropriate treatment was added. The plate layout for all free-drug experiments was kept consistent and is illustrated below (Figure 13). The control was complete growth media alone and the vehicle control (VC) was complete growth media plus the solvent used to dissolve the drug (DMSO). To obtain the IC50 concentrations to be used for encapsulation at each time point, the SK-N-BE(2) cells were treated with the experimental concentrations detailed in Section 2.7.

Following incubation at the two different time points, the plates were removed from the incubator and placed in the laminar flow where MTT solution was added to each well, making sure the plate was not exposed to direct light as MTT is light-sensitive. The plates were placed back into the incubator and incubated in the dark for approximately 4 hours. Following the 4-hour incubation, the assay was stopped by aspirating all the media in each well and adding DMSO to solubilise the fromazan product. Subsequently the plates were then read using a Promega GloMaxTM Multiscan Plate Reader to obtain optical density (OD) readings at a wavelength of 560 nm. These OD readings were used to calculate the cell viability and construct the dose-response curves.

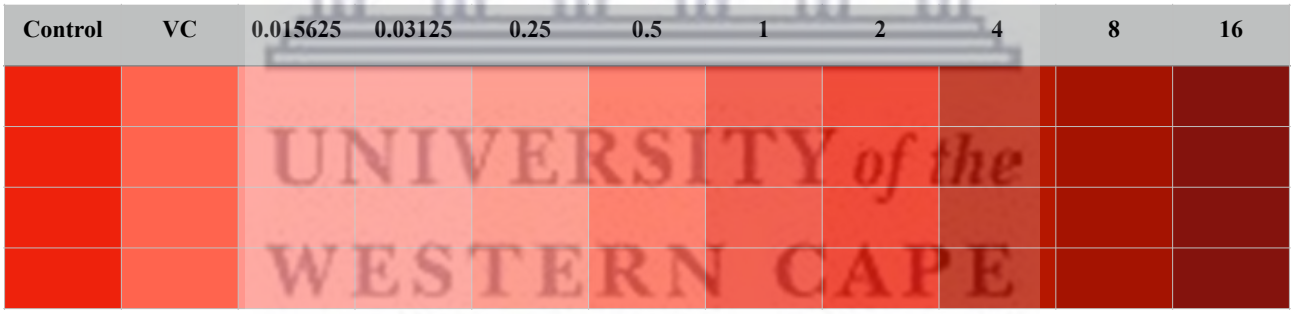

Figure 13: MTT assay plate layout showing the order of the concentrations and amount of treatments per plate.

2.8.3 Drug Encapsulated Experiments

Once the IC_{50} concentrations were calculated and confirmed, they were encapsulated in the nanoparticles via the steps outlined in Section 2.6.1. SK-N-BE(2) cell viability was then tested following exposure to these DX-CS-ALG and unloaded CS-ALG nanoparticles at log_{10} concentrations: 10µg/ml, 1µg/ml, 0.1µg/ml, and 0.01µg/ml. The steps carried out were in line with

those mentioned in Section 2.8.2. The plate layout below in Figure 14 illustrates the general layout of the DX-CS-ALG (A) and CS-ALG (B) experiments.

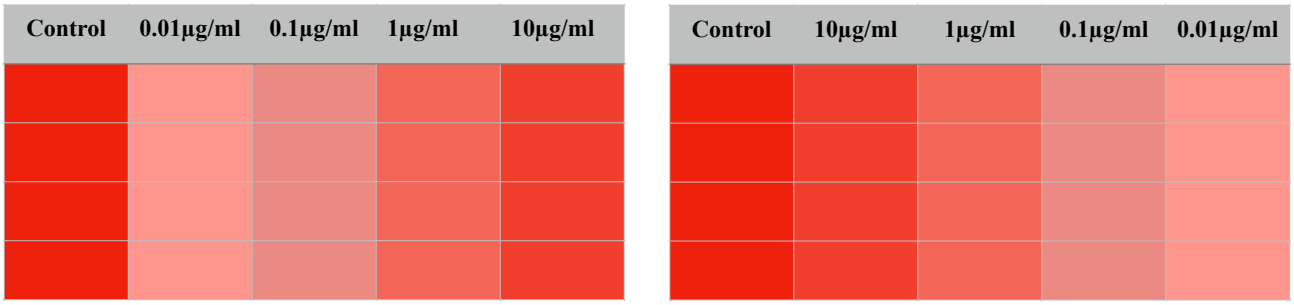

Figure 14: MTT assay plate layout showing the order of the concentrations and amount of treatments per plate for DX-CS-ALG (A) and CS-ALG (B) nanoparticles .

2.9 Reactive Oxygen Species Assay

Reactive oxygen species (ROS) are chemically reactive oxygen-containing molecules that are induced as a natural byproduct of oxygen metabolism. ROS are constantly produced and eliminated under normal physiological conditions, and have significant roles in cell signalling, homeostasis, and clearance of microbial infections (Freemerman et al., 2014). During times of environmental stress such as exposure to heat and ultraviolet light, or during infection, ROS levels can increase dramatically leading to oxidative stress. This oxidative stress can result in damage to cellular proteins, lipids, and DNA. Some examples of ROS include superoxide ions and peroxides (Freemerman et al., 2014).

2.9.1 ROS Reagent Preparation and Protocol

For the purpose of this assay, cells were seeded at a density of $1x10^5$ cells per ml. Following seeding, the SK-N-BE(2) cells were allowed to attach for 24 hours under normal growth conditions. Once the cells had attached, the growth media was aspirated from each well and the appropriate treatment was added. The plate layout below in Figure 14 illustrates the general layout of the experiment, with the positive control being 20% H_2O_2.

ROS assay stain was prepared by mixing the concentrate in the vial with 40µl of DMSO to produce a 500X stock solution. This stock solution was diluted further to produce a working stock at a concentration of 1X. Before adding the stain, the positive control was added to the wells and

incubated for 10 minutes. Following the 10-minute incubation, all media and the positive control were carefully removed from the respective wells. Next, 100µl of the ROS stain was added to each well and the plate was incubated for an hour. Following the 1 hour incubation, the stain was aspirated from each well and 100µl of PBS was added. The plate was then read immediately at 520nm.

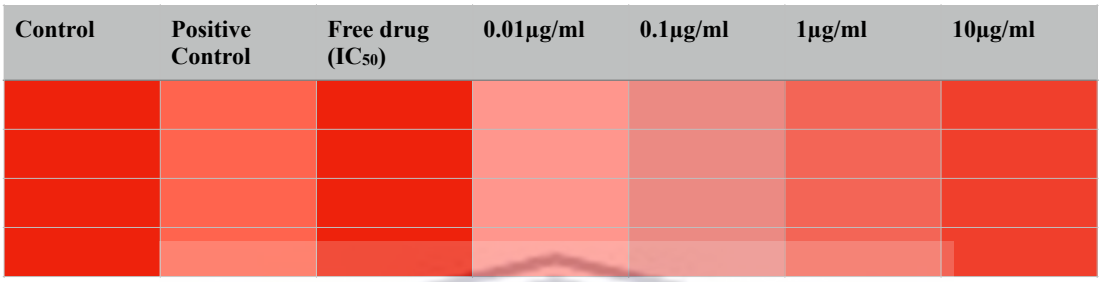

Figure 15: ROS assay plate layout. Positive control - 20% H_2O_2 and free drug - IC_{50}

2.10 Statistical Analysis

The growth curve as well as data correction was carried out using Microsoft Excel. Data obtained for ROS production, and cell viability effects of doxorubicin and DX-CS-ALG nanoparticles on SK-N-BE(2) cells were assessed for normality and analysed using One-Way ANOVA and the independent t-test if parametric, or using the Kruskal–Wallis test or Mann-Whitney test if non-parametirc. (GraphPad Prism version 7.01 for Windows, GraphPad Software, San Diego California USA, www.graphpad.com). Best-fit IC_{50} values were obtained from the dose-response curves also generated on GraphPad Prism. These IC_{50} values were tested and confirmed.

In the present study, SK-N-BE(2) neuroblastoma cells were exposed to doxorubicin and doxorubicin loaded nanoparticles in a log dose manner. A normal growth curve for SK-N-BE(2) cells was generated to examine their behaviour under normal culture conditions. A carefully designed study was conducted to ascertain the degree of potency for doxorubicin loaded nanoparticles, and free doxorubicin on the neuroblastoma cells. The sections below will provide more detail on the results obtained.

Chapter 3
Results and Discussion

In this chapter, the results of the research undertaken in this study are discussed.

3.1 Growth Curve

The SK-N-BE(2) neuroblastoma cell line was established in November of 1972 from a bone marrow biopsy taken from a child with disseminated neuroblastoma after repeated courses of chemotherapy and radiotherapy. SK-N-BE(2) cells exhibit moderate levels of dopamine beta-hydroxylase activity with cellular morphology varying. Some cells have long processes and others are epitheloid-like. When growing, these cells tend to aggregate, form clumps and float, a process more commonly known as sprouting (Atcc.org, 2019).

The growth curve illustrated in Figure 16 depicts a typical growth curve for the time points of the experiment, in which only the lag and log phase are demonstrated. A plateau phase was not reached as the cells may have needed more time to grow as demonstrated in a study carried out by Challagundla et al. in 2015, where cells only reached the plateau phase following 96 hours of growth. Thus it may be assumed that the growth curve obtained in the present study was in accordance with those reported in previous research.

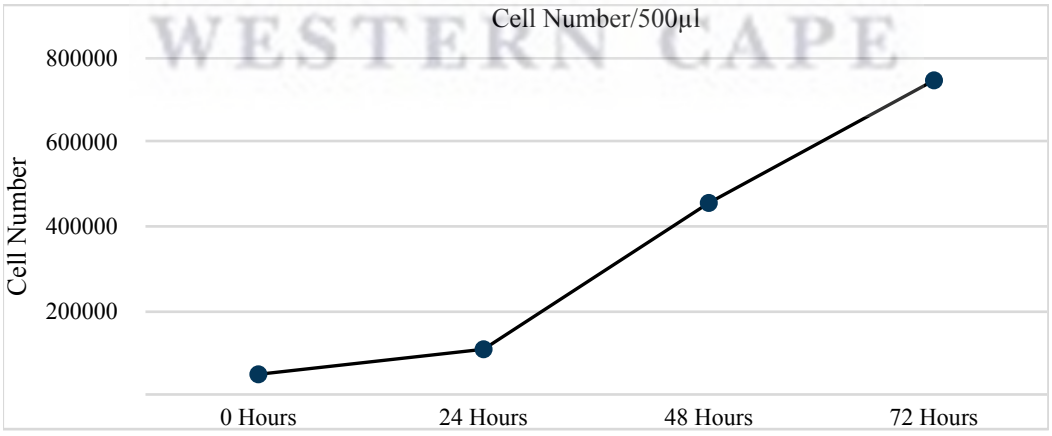

Figure 16: Growth curve of SK-N-BE(2) neuroblastoma cells under normal culture conditions. The Population Doubling Time (PDT) for the cells was calculated at 39.11 hours.

3.2 Nanoparticle Characteristics

3.2.1 Dynamic Light Scattering and Zeta Potential of Unloaded Nanoparticles

Dynamic Light Scattering (DLS) was used to determine the hydrodynamic size and polydispersity index, and measurements of 4 separate batches (experiments 1-4) were recorded and summarized in Table 6. CS-ALG nanoparticles demonstrated comparable average size and PDI measurements across each experiment, with a calculated average size and PDI of 363.7nm and 0.245, respectively. The zeta potential (ZP), an indication of surface forces, was also measured for each generated batch and summarized in Table 6. Notable batch-to-batch consistency was observed, with an average ZP of -41.8mV across each experiment.

Table 6: Hydrodynamic size, polydispersity index, and zeta potential of the CS-ALG nanoparticles.

Experiment	Size	PDI	ZP
CS-ALG Experiment 1	391,6	0,316	-37,2
	367,4	0,231	-36,9
	369,1	0,265	-36,8
Average	376,0	0,271	-37,0
CS-ALG Experiment 2	384,9	0,241	-45,6
	385,9	0,273	-43,8
	389,1	0,272	-43,3
Average	386,6	0,262	-44,2
CS-ALG Experiment 3	314,7	0,232	-44,2
	311,2	0,187	-44,3
	301,5	0,175	-44,9
Average	309,1	0,198	-44,5
CS-ALG Experiment 4	389,0	0,217	-42,3
	375,0	0,259	-41,7
	384,6	0,267	-41,1
Average	382,9	0,248	-41,7
Total Average	363,7	0,245	-41,8

3.2.2 Dynamic Light Dynamic Light Scattering and Zeta Potential of Loaded Nanoparticles

Dynamic Light Scattering (DLS) was used to determine the hydrodynamic size and polydispersity index of loaded nanoparticles, and measurements of 4 separate batches (experiments 1-4) were recorded and summarized in Table 7. DX-CS-ALG nanoparticles demonstrated comparable average size and PDI measurements across each experiment, with an average size and PDI of 361.2nm and 0.260, respectively. The zeta potential (ZP), an indication of surface forces, was also measured for each generated batch and summarized in Table 7. Notable batch-to-batch consistency was observed, with an average calculated ZP of -39.6mV across each experiment.

Table 7: Hydrodynamic size, polydispersity index, and zeta potential of the DX-CS-ALG nanoparticles.

	Size	PDI	ZP
DX-CS-ALG Experiment 1	377,8	0,365	-37,2
	380,8	0,354	-37,1
	403,6	0,477	-40,1
Average	387,4	0,399	-38,1
DX-CS-ALG Experiment 2	367,4	0,145	-39,9
	351,6	0,242	-40,4
	357,2	0,175	-39,3
Average	358,7	0,187	-39,9
DX-CS-ALG Experiment 3	385,6	0,237	-42,9
	376,7	0,160	-40,3
	400,3	0,379	-43,0
Average	387,5	0,259	-42,1
DX-CS-ALG Experiment 4	311,6	0,159	-38,7
	306,8	0,225	-37,9
	315,4	0,203	-38,0
Average	311,3	0,196	-38,2
Total Average	361,2	0,260	-39,6

One of the most effective ways to synthesise NPs is to use ultrasonic waves. In sonochemistry, the most appropriate frequency range has been identified as being anywhere between 20 kHz to 1 MHz (Schroeder, Kost and Barenholz, 2009). Throughout long-term and high-power sonication, a considerable amount of energy is released, ultimately affecting particle size. To this extent, ultrasonication is one of the most common methods used in the production of polymeric NPs. By

sonication, aggregates can be crushed, leading to smaller nanoparticle sizes and more uniform PDIs (Büyük et al., 2020).

An optimisation study for chitosan nanoparticles carried out by Büyük et al., (2020) demonstrated that the optimum conditions required for producing ideal nanoparticles (smallest sizes, with uniform PDIs and stable ZPs) were a sonication time of 5 minutes at 50W, chitosan concentration of 4mg/ml, cross linker (TPP) concentration of 2mg/ml, and a mass ratio (chitosan:TPP) of 5:1. Using these parameters, they prepared batches of unloaded NPs and NPs loaded with bovine serum albumin (BSA). Their NP sizes ranged from 115.0nm (unloaded) to 233.3nm (loaded), with PDIs of 0.360 (unloaded) and 0.450 (loaded). The results obtained in the present yielded NPs with a slightly bigger size, however they had better dispersity. These differences could be due to the crosslinking agent used, the mass ratio, and the loaded substance (Büyük et al., 2020).

Particle size and surface charge are two vital factors taken into account when designing controlled drug delivery systems. A similar NP delivery system to the present study was designed in 2017 for the oral delivery of naringenin in diabetic animals (Maity, Mukhopadhyay, Kundu and Chakraborti, 2017). Their results demonstrated that the optimal CS:ALG mass ratio is between 2:1 And 3:1, which is in line with the mass ratio selected in the present study. They considered this range optimum because the particles synthesised illustrated appropriate size ranges (224.6nm and 216.4nm) with minimum PDI (0.340 and 0.390). Whilst the size of the NPs synthesised in the present study are slightly bigger, their dispersity remains better. However, both studies have shown that CS-ALG nanoparticles synthesised via sonication exhibit highly negative zeta potentials. This serves as a confirmation of the presence of alginate in the system. The ZP values also improve stability and provide effective protection against self-aggregation (Mukhopadhyay et al., 2015).

3.3 Transmission Electron Microscopy

Since research in nanotechnology turned its attention to the biomedical field, the development of new nanoproducts has involved the study of their interactions with their surrounding environments. The knowledge of their functional and structural interactions with cells, tissues, and organs is a vital key to understanding their safety and efficacy (Malatesta, 2021). *In vivo* imaging techniques such as magnetic resonance imaging, optical imaging, and positron emission tomography have been used

extensively, frequently in combination, to establish nanoparticle targeting, biodistribution, and clearance from organisms (Karaman, Sarparanta, Rosenholm and Airaksinen, 2018).

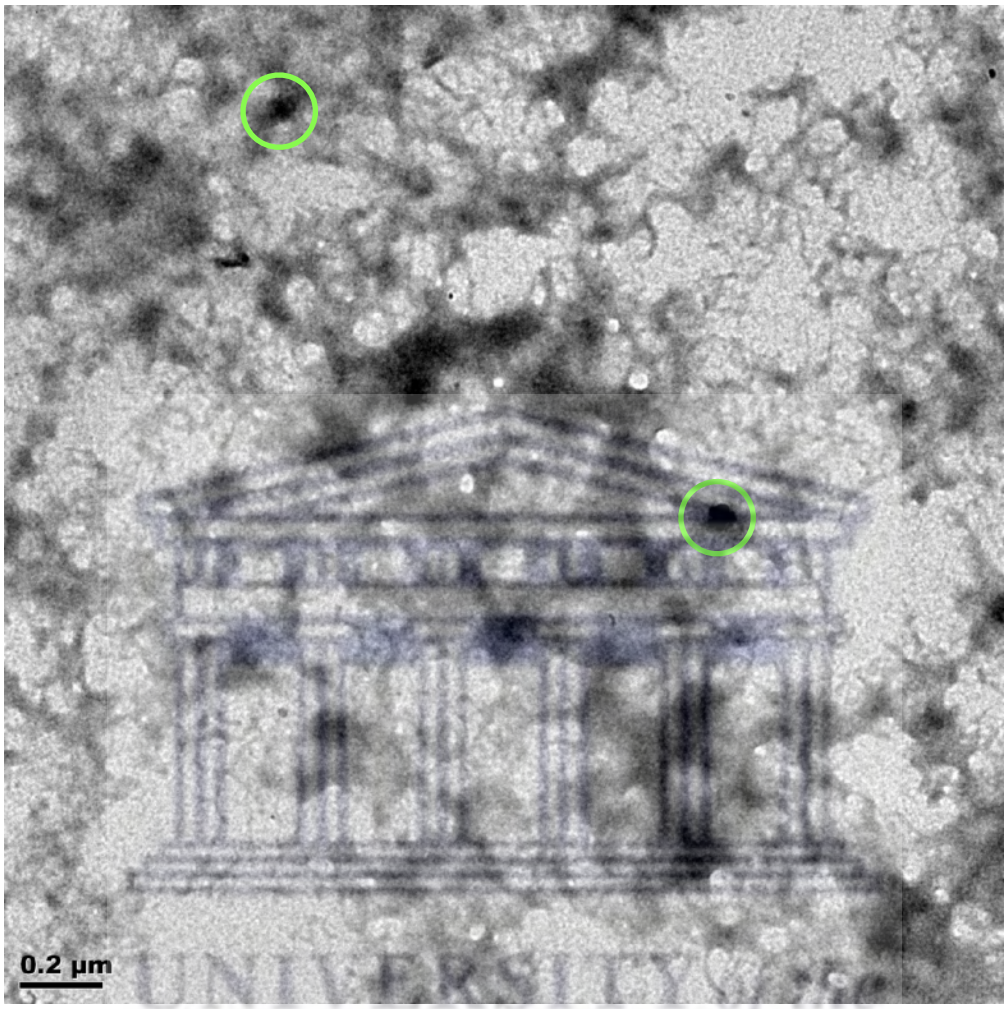

Figure 17: TEM of CS-ALG nanoparticles.

TEM confirmed the presence of nanoparticles and provided morphological information of typical CS-ALG nanoparticles. Figure 17 shows two possible nanoparticles from the sample, the particle sizes can be estimated to be about 100nm, significantly smaller than the sizes estimated using DLS. However, the nanoparticles do not show a smooth, uniform surface but a fluffy appearance. This fully appearance in addition to the aggregating nature of these nanoparticles could be a possible explanation to the bigger size values obtained using DLS. Images obtained in a previous study exhibit similar characteristics to those obtained in the present study, however the images obtained by Dai et al. display smaller nanoparticles which are more compact (see Appendix 1).

3.4 24 and 48-Hour Doxorubicin Cell Viability

The SK-N-BE(2) cells were treated with varying concentrations of Dox over 24 and 48-hour time intervals and percentage viability was determined using the MTT assay (Figure 18). Following 24 hours of exposure, there was an overall significant difference among the means ($p<0.05$), with significant ($p=0.0191$ [*], $p=0.0021$ [**], $p<0.0001$ [****]) differences at a concentration of 0.25, 1 µM and 2-16 µM, respectively. Following 48 hours of exposure, there were notably highly significant ($p<0.0001$ [****]) differences at concentrations between 0.25-16µM, respectively.

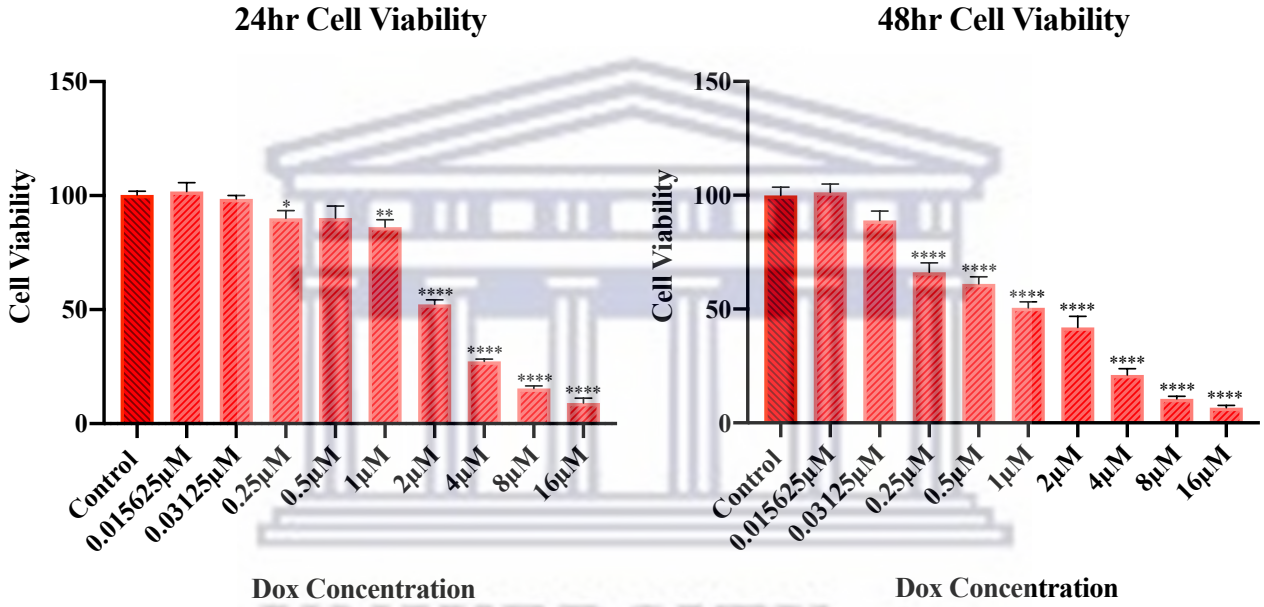

Figure 18: Cell viability following 24 and 48 hours of exposure to Dox.

Stress-protective heat shock proteins (HSPs) are often over-expressed in neoplastic tissues and cancer cell lines. In 2007, Zanini et el. illustrated that neuroblastoma cells are able to defend against the cytotoxic effects of doxorubicin until HSPs are up-regulated. In their study, they illustrated that time-dependent HSP response peaked after 6 hours following exposure to 1nmol/L of doxorubicin. To a certain extent, the results of the present study concur with those observed by Zanini et el., as their study illustrated that AF8, IMR-5, and SJ-N-K neuroblastoma cells had no decreases in heat shock protein levels or any appreciable anti-proliferative effect following exposure to 1nmol/L of doxorubicin, which is in accordance with the present study, which shows decreases in cell viability at concentrations greater than 1nmol/L. In addition, increased doxorubicin concentrations caused a progressive decrease in heat shock protein expression and an anti-proliferative effect. Their results

concluded that a concentration higher than 1nmol/L of doxorubicin alone would be needed to cause an anti-proliferative effect which is in line with the findings of the present study which show significant decreases in viability at concentrations greater than 0.25µM. With regards to the present study, it can be tentatively concluded that the cytotoxic effect of doxorubicin on SK-N-BE(2) follows a similar mechanism but further investigations are required to draw a definitive conclusion.

Similarly, whilst the results of the present study concur with those found by Zanini et el. (2007), they are also in accordance with those found by Rebbaa et el. in 2003. Their study illustrated that rapid cell death was observed after exposure to 10^{-6} M and 10^{-5} M of doxorubicin, whilst those exposed to 10^{-7} M experienced irreversible growth arrest with signs indicative of senescence. Senescence-associated-*β*-galactosidase (SA-*β*-gal) staining after 5 days of incubation with doxorubicin confirmed that these cells had acquired a senescent phenotype. In order to definitively conclude the possibility of senescence, a similar staining technique will need to be conducted (Reba et al, 2003).

In 2018, a study demonstrated the combined effect of curcumin and doxorubicin on SH-SY5Y neuroblastoma cells. Their results demonstrated that a doxorubicin concentration of 5µg/ml decreased cell viability by approximately 50% (Namkaew et al, 2018). However, in the present study a slightly lower concentration achieved 50% cell viability. One possible explanation for the differences observed could be the cell line used. SH-SY5Y cells are a thrice sub-cloned cell line derived from the SK-N-SH neuroblastoma cell line, whilst SK-N-BE(2) cells are not a sub-cloned cell line.

3.4.1 Determination of Doxorubicin IC_{50} Concentration

Figure 19a illustrates the dose-response curve and the possible IC_{50} cell viability graphs after 24 hours of exposure. Following 24 hours of exposure, an IC_{50} value of 2.381µM was calculated for doxorubicin. It must be noted, however, that subsequent testing of the calculated IC_{50} value yielded approximate cell viability of 58%. Consequently, the concentration of doxorubicin was increased slightly to 2.5µM and 3µM, which resulted in approximately 60% and 48% cell viability respectively. Therefore, a concentration of 3µM was selected for the 24-hour encapsulation experiments. Following 48 hours of exposure (Figure 19b), doxorubicin had an IC_{50} value of 0.9173 µM, which when tested reduced viability to approximately 49%. Thus, the calculated IC_{50} value for 48 hours of exposure was confirmed.

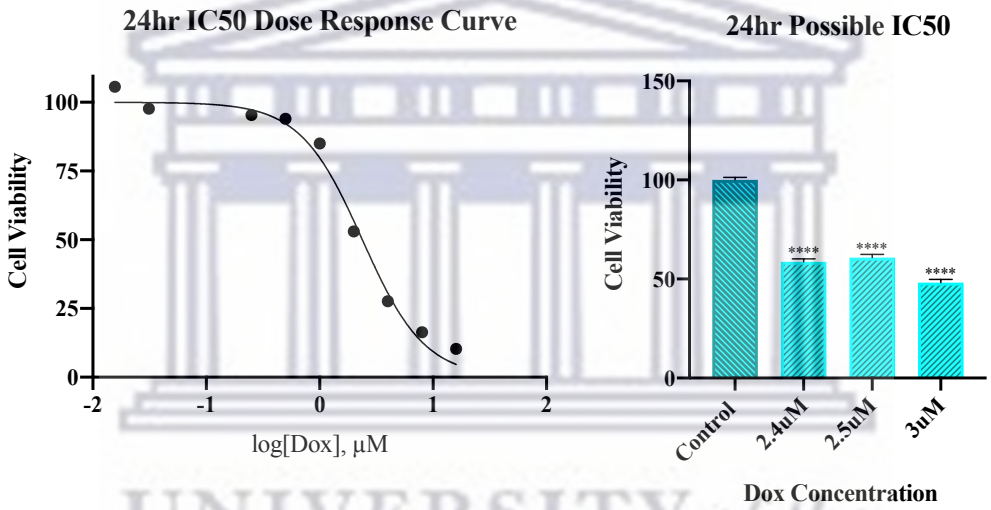

Figure 19a: 24-hour dose response curve and possible IC_{50} cell viabilities.

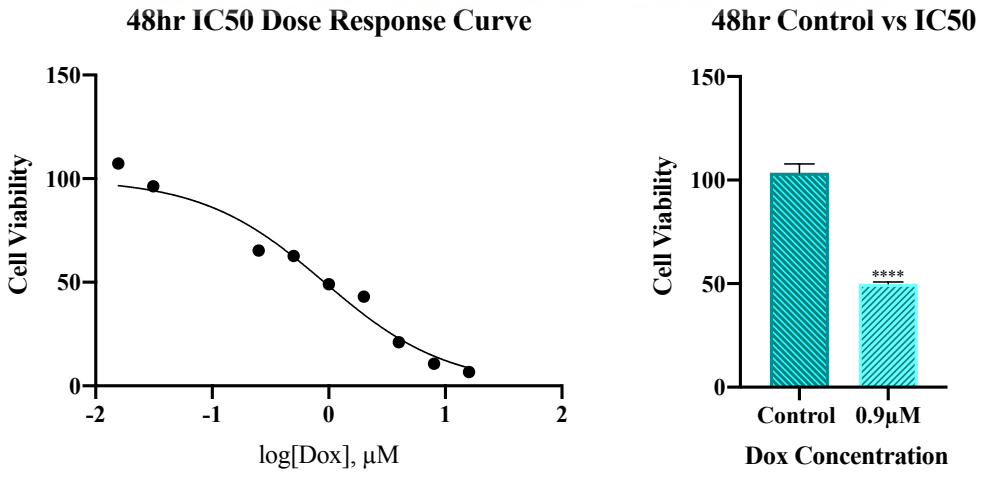

Figure 19b: 48-hour dose response curve and possible IC_{50} cell viabilities.

3.5 Doxorubicin Encapsulation Efficiency

Following the confirmation of the IC_{50} concentrations for each time point, these concentrations were loaded in the DX-CS-ALG nanoparticle experiments. Nanoparticles were loaded with 3µM and 0.9µM of doxorubicin for the 24 and 48-hour time points respectively, and encapsulation efficiency was determined. Remarkably, an average encapsulation efficiency of 86% was achieved for nanoparticles loaded with 3µM of doxorubicin, however those loaded with 0.9µM of doxorubicin had an encapsulation efficiency of 66% . The straight line graph depicted in Figure 20 was used in combination with the equation described in Chapter 2: Section 2.6.4.

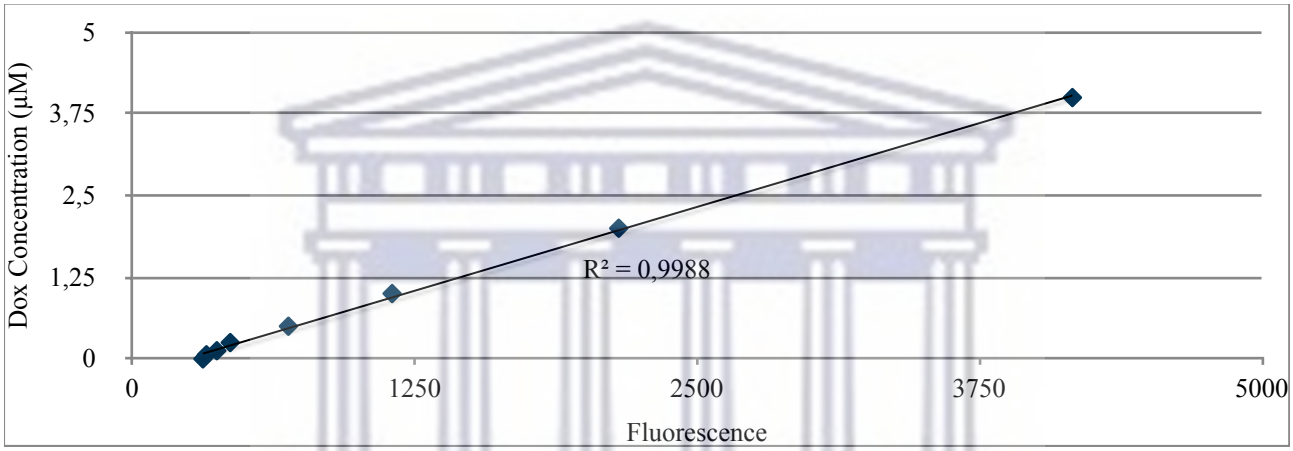

Figure 20: Straight line graph used to predict doxorubicin encapsulation efficiency

3.6 Nanoparticle Quantification

Following synthesis, nanoparticles were purified, frozen at -80°C, freeze-dried, and the powdered nanoparticles were subsequently weighed. Measurements were recorded for 4 separately synthesized batched and summarized in Table 8. An average calculated yield of 875µg was recorded across each of the reported measurements.

Table 8: Weighed particles per experiment

	1	2	3	4	Average
	35ml	35ml	35ml	35ml	
Weighed Particles (mg)	0,7	0,8	1,0	1,0	0,875
Particles per ml	0,02	0,02	0,03	0,03	0,03

3.7 24 and 48-Hour Unloaded Nanoparticle Cell Viability

The SK-N-BE(2) cells were exposed to varying concentrations of unloaded nanoparticles over 24 and 48-hour time intervals. Following both 24 and 48-hour exposure periods, no significant differences were observed at each of the presently tested nanoparticle concentrations.

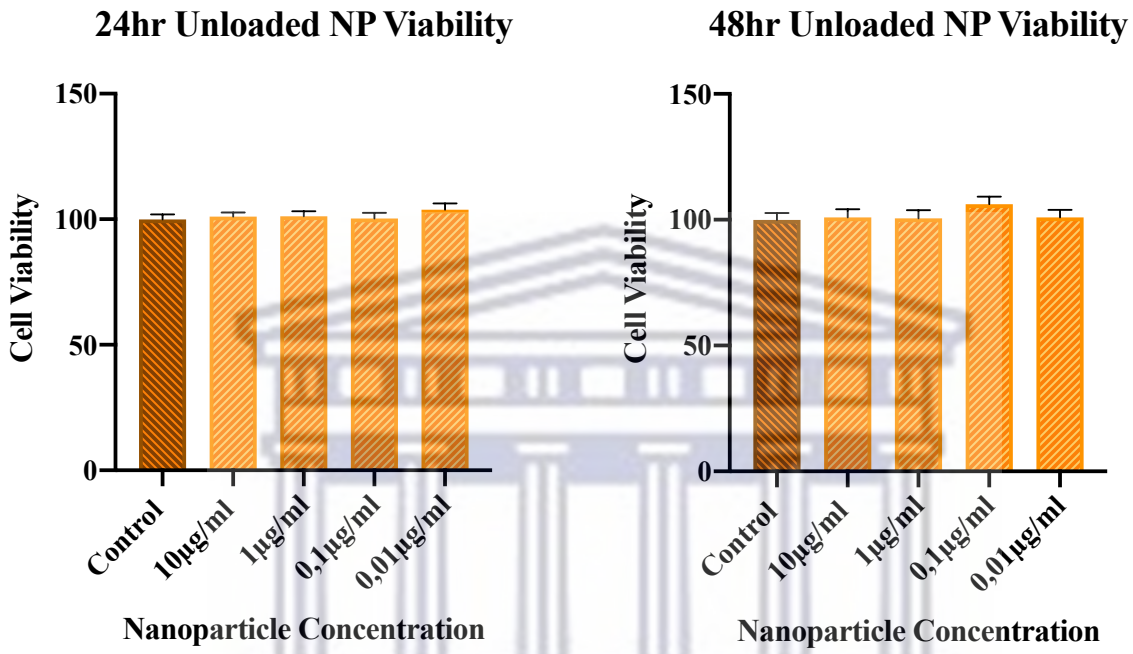

Figure 21: Cell viability following 24 and 48 hours of exposure to unloaded nanoparticles.

The results illustrated in Figure 21 suggest that chitosan-alginate nanoparticles are highly biocompatible, as they do not decrease viability following exposure over 24 and 48 hours. A study carried out Rafiee et al., (2014) demonstrated similar viability results. Interestingly, the cells in their study seemed to proliferate quicker when treated with chitosan, alginate, or both over 4 and 24-hour periods. A possible explanation of their results could be due to the influence of mitochondrial activity in the cells stimulating them to proliferate (Dupuy et al., 1994).

Similarly, the results obtained in the present study align with those obtained by Yoncheva et al., (2020) in which they designed a doxorubicin drug delivery system using chitosan-alginate nanoparticles. In their study, they treated L5178 MDR1 cells and H9c2 cardioblasts with doxorubicin, doxorubicin-loaded nanoparticles, and unloaded nanoparticles for 24 hours. Their

results also showed no significant decreases in cell viability across both cell lines with unloaded nanoparticles.

3.8 24 and 48-Hour Doxorubicin Loaded Nanoparticle Viability

Similarly, the SK-N-BE(2) cells were exposed to varying concentrations of nanoparticles loaded with the confirmed IC_{50} concentrations for the 24 and 48-hour time intervals. Following both 24 and 48-hour exposure periods, no significant differences were observed at each of the presently tested nanoparticle concentrations.

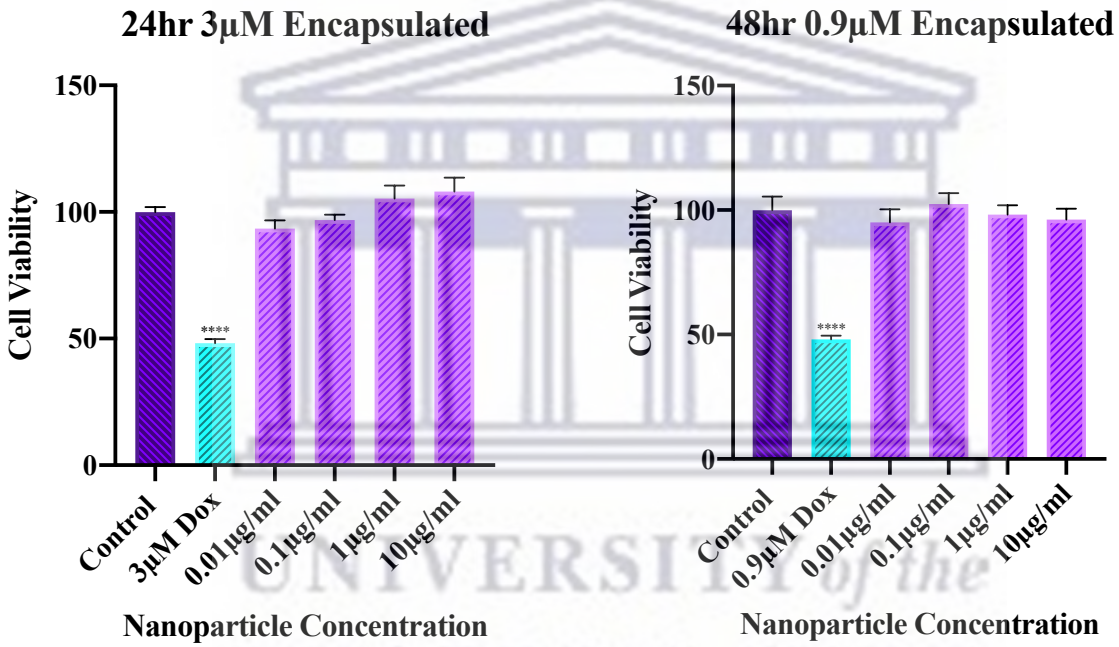

Figure 22: Cell viability following 24 and 48 hours of exposure to doxorubicin IC_{50} and loaded nanoparticles.

The results illustrated in Figure 22 suggest there is insufficient release of doxorubicin from the loaded nanoparticles across the various concentrations. The release of doxorubicin from the CS-ALG hydrogel is strongly dependent on its ability to absorb water, and this ultimately depends on the amount of sodium alginate present in the CS-ALG nanoparticle complex. A study by Wu et al., (2020) demonstrated how different CS-ALG compositions affected water absorption and drug release. In their study, they tested three different CS-ALG weight ratios, (1:2, 1:3, and 1:4) and concluded that hydrogel beads composed in a 1:4 ratio had the greatest degree of swelling and water

uptake. A possible explanation for this may be due to the lower cross-linking density of the CS-ALG network. The ratio used in the present study was 2:1 and thus could have led to a denser cross-linked network ultimately affecting its water absorption. Additionally, Wu et al., (2020) demonstrated that environments with an increased pH assist in the degradation and release of doxorubicin from CS-ALG complexes.

3.9 Cellular Morphology Following Exposure to Loaded Nanoparticles

This section will illustrate cellular morphology pictures taken following exposure of the neuroblastoma cells to the various nanoparticle concentrations for 24 and 48 hours.

3.9.1 24-Hour Morphology

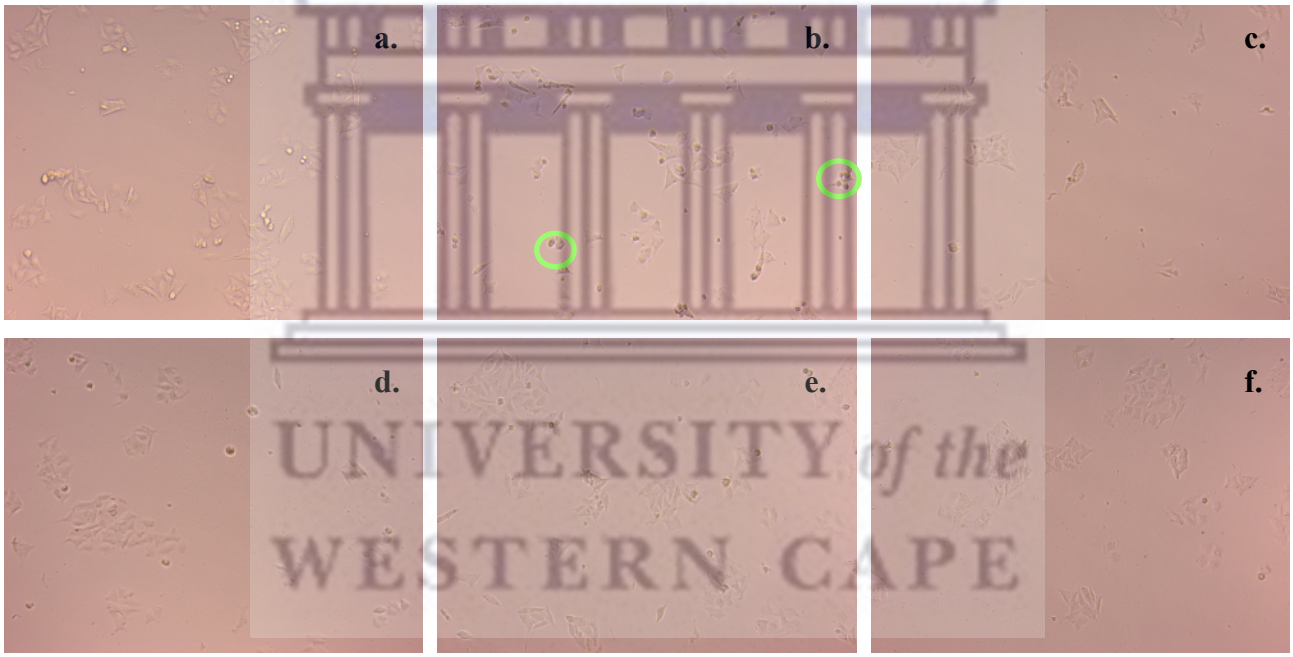

Figure 23: Cell morphology after 24 hours of exposure to doxorubicin IC_{50} and DX-CS-ALG nanoparticles. (**a** = control, **b** = doxorubicin IC_{50} (3 µM), **c** = 0.01 µg/ml, **d** = 0.1 µg/ml, **e** = 1 µg/ml, and **f** = 10 µg/ml)

Figure 23 depicts SK-N-BE(2) cell number and cellular morphology following exposure to the confirmed IC_{50} doxorubicin concentration and various DX-CS-ALG nanoparticle concentrations for 24 hours. The pictures are labelled starting with the control, followed by the free doxorubicin IC_{50} concentration, and finally the different concentrations of nanoparticles. When compared to the control, the morphology of the cells exposed to the free doxorubicin IC_{50} concentration exhibit

signs of cell death and apoptosis (circled in green) in addition to a decrease in cell number. However, all concentrations of loaded nanoparticles seem to have no significant effect on cellular morphology and overall cell number. These results are supported by the values obtained in the MTT viability assay. Explanations for the possible reasons are discussed in the section above (Section 3.9).

3.9.2 48-Hour Morphology

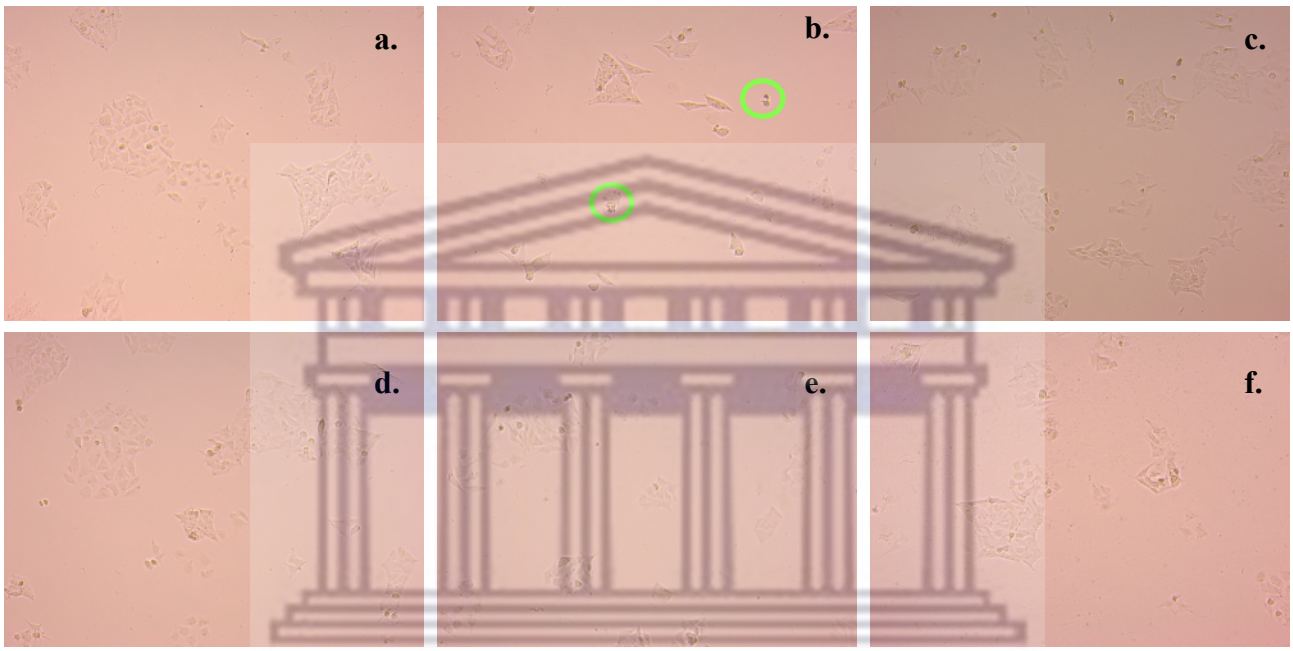

Figure 24: Cell morphology after 48 hours of exposure to doxorubicin IC_{50} and DX-CS-ALG nanoparticles. (**a** = control, **b** = doxorubicin IC_{50} (0.9 µM), **c** = 0.01 µg/ml, **d** = 0.1 µg/ml, **e** = 1 µg/ml, and **f** = 10 µg/ml)

Figure 24 depicts SK-N-BE(2) cell number and cellular morphology following exposure to the confirmed IC_{50} doxorubicin concentration and various DX-CS-ALG nanoparticle concentrations for 48 hours. The pictures are labelled in a similar manner starting with the control, followed by the free doxorubicin IC_{50} concentration, and finally the different concentrations of nanoparticles. When compared to the control, the morphology of the cells exposed to the free doxorubicin IC_{50} concentration exhibit signs of cell death and apoptosis (circled in green) in addition to a decrease in cell number. However, all concentrations of loaded nanoparticles seem to have no significant effect on cellular morphology and overall cell number. These results are supported by the values obtained in the MTT viability assay. Explanations for the possible reasons are discussed in the section above

(Section 3.9). Cellular morphology showing apoptosis and senescence following exposure to doxorubicin can be seen in Appendix 2.

3.10 Reactive Oxygen Species Assay

The graphs depicted in Figure 25 illustrate ROS production following 24 and 48 hours of incubation with the various nanoparticle concentrations and the free doxorubicin IC_{50}. The results obtained are in line with those produced in the viability assays and the cellular morphology pictures. When compared to the control, there are no significant differences in ROS production across all nanoparticle concentrations and the free doxorubicin IC_{50}.

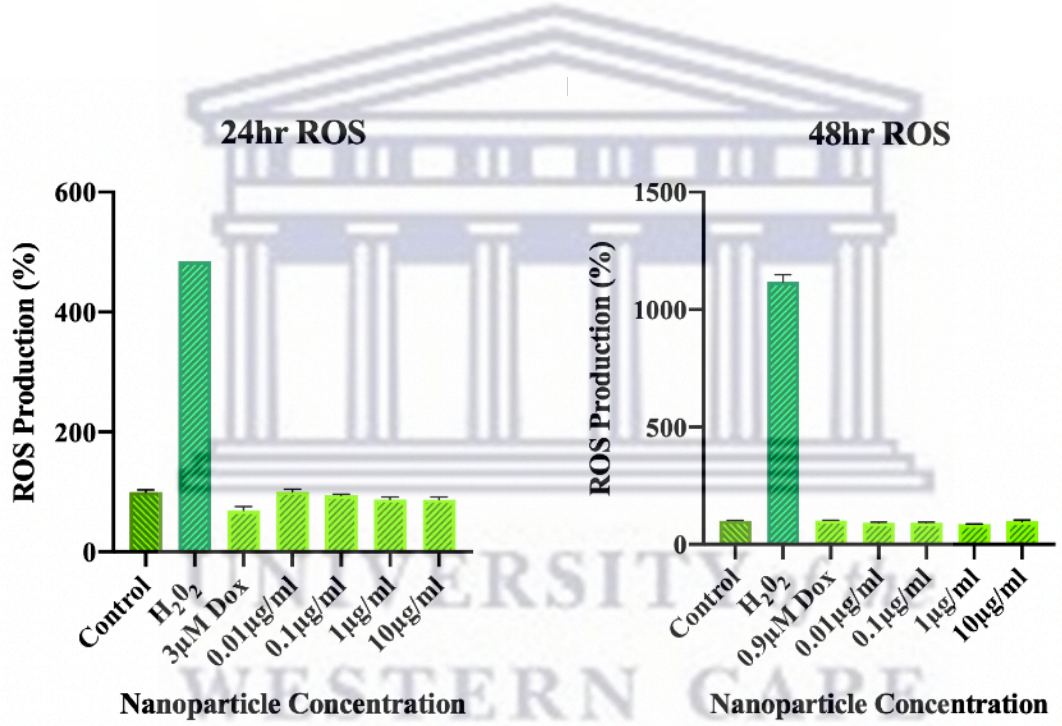

Figure 25: ROS production following 24 and 48 hours of exposure to doxorubicin IC_{50} and loaded nanoparticles.

Doxorubicin is a powerful anti-tumoral drug used in the treatment of various cancers. A study by Pilco-Ferreto and Calaf (2016) demonstrated the influence of doxorubicin in apoptosis and oxidative stress in MCF-10F, MCF-7, and MDA-MB-231 breast cancer cell lines. Their study concluded that doxorubicin decreased anti-apoptotic Bcl-2 protein expression, however it increased oxidative stress by increasing the production of hydrogen peroxide, whilst simultaneously decreasing NF-κB gene and protein expression in MCF-7, a tumorigenic triple-positive cell line.

Similarly, their results demonstrated that doxorubicin-induced apoptosis in MDA-MB-231 by increasing BAX, caspase 8, and caspase 3 production, whilst also decreasing Bcl-2 protein expression. Ultimately their results concluded that doxorubicin was able to influence ROS damage in these two cell lines. The results of the present study are not inline with those obtained by Pilco-Ferreto and Calaf (2016), as there is no indication of ROS production across all concentrations and the free IC_{50}. A possible explanation for the variation in results could be the cell line used. However, due to the insufficient release of doxorubicin from the nanoparticles, it is expected that ROS production will be impaired as there were no significant decreases in viability across all concentrations.

Chapter 4
Conclusion

Nanotechnology, the engineering and manufacturing of materials using atomic and molecular components, is expected to benefit all branches of medicine, with oncology being one of the earliest and most beneficiary to date. The vascularity of tumors is highly diverse in character, ranging from areas distinguished by vascular necrosis to areas which are densely vascularised to aid in the adequate supply of oxygen and nutrients to growing tumors (Alexis et al., 2008). Tumor blood vessels have several abnormalities when compared to normal blood vessels, including a high proportion of proliferating endothelial cells with abnormal underlying basement membranes, increased tortuosity of blood vessels, and a deficiency in pericytes (Jain, 2012). Additionally, tumor microvessels demonstrate enhanced permeability partially caused by the irregular secretion of vascular endothelium growth factor, nitric oxide, matrix metalloproteinases, prostaglandins, and vascular endothelium growth factor (Jain, 2012).

The transport of macromolecules into tumors via their microvasculature may occur through open endothelial junctions or transendothelial channels. The pore cutoff size of these pathways in numerous models has been roughly estimated to be less than 1000nm, with a study showing the *in vivo* extravasation of liposomes into tumor xenografts having a cutoff size in the 400nm range (Yuan et al., 1995). In general, the extravasation of nanoparticles is inversely proportional to its size, thus suggesting smaller nanoparticles, less than 200nm in size, would be most effective for extravasating tumor microvasculature (Kong, Braun, and Dewhirst, 2000). The tumor lymphatic system is also known to have abnormal characteristics, resulting in fluid retention and high interstitial pressures with an outward connective interstitial fluid flow (Alexis et al., 2008). Ultimately, the leaky microvasculature and lack of an intact lymphatic system results in an enhanced permeation and retention (EPR) effect and a “passive” cancer-targeting treatment via the build-up of nanocarrier systems in the tumor at considerably higher concentrations compared to the plasma and surrounding tissues (Maeda et al., 2000).

The hypothesis that the synthesised DX-CS-ALG nanoparticle system will have a greater antagonistic effect than free doxorubicin on SK-N-BE(2) cell proliferation and morphology *in vitro* is not accepted in the present study. As shown in the results, there were no significant decreases in cell viability across all tested concentrations when the SK-N-BE(2) cells were exposed to the DX-

CS-ALG nanoparticles over both 24 and 48-hour incubation periods. These results were supported by the morphology seen, as changes were only observed in cells exposed to the free IC_{50}. All remaining objectives for the study were met.

4.1 Limitations of The Study

The present study is limited to a single neuroblastoma cell line, SK-N-BE(2) cells. The strength of the findings could have been improved by possibly adding a different variation of neuroblastoma cells such as UKF-NB-3, UKF-NB-6 and IMR-32. Every effort was made to study the effect of different chitosan to alginate weight ratios, and how this would affect size, but due to time constraints brought on by the COVID-19 pandemic, only the single weight ratio was assessed. Variations in the size of nanoparticles tested may have shown different effects on cell viability and morphology. Additionally, the present study did not focus on any drug release studies to evaluate the rate at which doxorubicin is released from the nanoparticle system. Polymeric nanoparticle delivery systems can be designed to release encapsulated drugs through diffusion, swelling, or bulk/ surface erosion, followed by further diffusion in a time or condition dependant manner. The release of the active agent may be constant or cyclic over extended periods, or it may be triggered by environmental or other external events (Kost and Langer, 2012). Finally, the study did not focus on any possible mutations that may have occurred throughout the experimental period which may have led to increased resistance against the DX-CS-ALG nanoparticle.

4.2 Future Directions and Prospective Studies

Combination therapy, a treatment modality that combines two or more therapeutic agents, is a cornerstone of cancer therapy (Yap, Omlin, and De Bono, 2013). The amalgamation of anti-cancer drugs enhances efficacy compared to the mono-therapy approach because it targets key pathways in a synergistic or additive manner (Albain et al., 2008). Drug synergism is an important research tool that can be exploited to develop more potent anticancer drug combinations that will eventually lead to better prognosis of malignant diseases and decreased cancer mortality rates. This approach may potentially reduce drug resistance in various cancers while simultaneously reducing tumor growth and metastatic potential (Mokhtari et al., 2017). An example of such a therapy involves a study carried out by Michaelis et al., (2008) in which they showed that that Cisplatin resistant neuroblastoma cells exhibit increased levels of EGFR receptors, thus by combining the two drugs

(Cisplatin and EGFR inhibitor II), a more efficacious effect may be seen in cell lines that may acquire resistance to certain drugs (in this case, Cisplatin).

A form of combination therapy can be accomplished by synthesising multilayer nano-delivery systems using a layer-by-layer (LbL) assembly. Polyelectrolyte multilayer capsules (PMCs) composed using an LbL approach of oppositely charged polyelectrolytes on sacrificial colloidal particles have been studied extensively for their possible applications in drug delivery, bio-sensing, catalysis, and micro-reactors (Kurapati and Raichur, 2012). To this extent, Ye et al., (2005) successfully synthesised a polysaccharide multilayer nanocapsule composed of chitosan and alginate on monodisperse polystyrene (PS) nanoparticles. In their study, they used an acridine hydrochloride (AH) drug model to investigate the loading and release properties of the nanoparticles. Their results demonstrated that the positively charged AH was spontaneously deposited into the capsule via the electrostatic interaction with the negatively charged styrene sulfonate residues in the PS nanoparticle template. Such nanocapsules made from natural polysaccharides demonstrate a promising potential in controlled drug release for cancer therapy.

Nanoparticle delivery systems can be further modified for "active" cancer targeting via the functionalisation of their surface with ligands such as peptides, antibodies, aptamers, or small molecules capable of recognising tumor-specific or tumor-associated antigens in the tumor microenvironment (Alexis et al., 2008). When nanocarriers target the extracellular portion of tumor membranes displaying specific antigens, they may be specifically taken up by cancer cells via receptor mediated endocytosis, with numerous studies successfully reporting this process (Kirpotin et al., 2006; Farokhzad et al., 2006; Chiu, Ueno, and Lee, 2004; Bagalkot et al., 2006). A schematic illustration demonstrating "passive" and "active" targeting of cancer cells can be seen in Appendix 3.

The specific targeting, intracellular uptake, and regulated therapeutic delivery on anticancer agents are characteristics obtained through the meticulous design of nanocarrier systems. Their application in cancer therapy is therefore an exciting and promising area of investigation.

References

Accord Healthcare. 2022. *Doxorubicin 2 mg/ml Concentrate for Solution for Infusion - Summary of Product Characteristics (SmPC) - (emc)*. [online] Medicines.org.uk. Available at: <https://www.medicines.org.uk/emc/product/6112/smpc#gref> [Accessed 21 May 2022].

Ackermann, S., Cartolano, M., Hero, B., Welte, A., Kahlert, Y., Roderwieser, A., Bartenhagen, C., Walter, E., Gecht, J., Kerschke, L. and Volland, R., 2018. A mechanistic classification of clinical phenotypes in neuroblastoma. *Science*, *362*(6419), pp.1165-1170.

Albain, K.S., Nag, S.M., Calderillo-Ruiz, G., Jordaan, J.P., Llombart, A.C., Pluzanska, A., Rolski, J., Melemed, A.S., Reyes-Vidal, J.M., Sekhon, J.S. and Simms, L., 2008. Gemcitabine plus paclitaxel versus paclitaxel monotherapy in patients with metastatic breast cancer and prior anthracycline treatment. *Journal of Clinical Oncology*, *26*(24), pp.3950-3957.

Alexis, F., Rhee, J.W., Richie, J.P., Radovic-Moreno, A.F., Langer, R. and Farokhzad, O.C., 2008, January. New frontiers in nanotechnology for cancer treatment. In *Urologic Oncology: Seminars and Original Investigations* (Vol. 26, No. 1, pp. 74-85). Elsevier.

Alshehri, S., Imam, S.S., Rizwanullah, M., Akhter, S., Mahdi, W., Kazi, M. and Ahmad, J., 2020. Progress of cancer nanotechnology as diagnostics, therapeutics, and theranostics nanomedicine: preclinical promise and translational challenges. *Pharmaceutics*, *13*(1), p.24.

Atcc.org. 2019. *SK-N-BE(2) ATCC ® CRL-2271™ Homo sapiens brain*. [online] Available at: https://www.atcc.org/products/all/CRL-2271.aspx#characteristics [Accessed 12 Nov. 2019].

Baker, D.L., Schmidt, M.L., Cohn, S.L., Maris, J.M., London, W.B., Buxton, A., Stram, D., Castleberry, R.P., Shimada, H., Sandler, A. and Shamberger, R.C., 2010. Outcome after reduced chemotherapy for intermediate-risk neuroblastoma. *New England Journal of Medicine*, *363*(14), pp.1313-1323.

Bleeker, G., Tytgat, G.A., Adam, J.A., Caron, H.N., Kremer, L.C., Hooft, L. and van Dalen, E.C., 2015. 123I-MIBG scintigraphy and 18F-FDG-PET imaging for diagnosing neuroblastoma. *Cochrane Database of Systematic Reviews*, (9).

Borriello, L., Seeger, R.C., Asgharzadeh, S. and DeClerck, Y.A., 2016. More than the genes, the tumor microenvironment in neuroblastoma. *Cancer letters*, *380*(1), pp.304-314.

Büyük, N.İ., PELİT, P., Derman, S., Mustafaeva, Z. and Yücel, S., 2020. An optimization study for chitosan nanoparticles: synthesis and characterization. *Celal Bayar University Journal of Science*, *16*(2), pp.119-127.

Cancer, C. 2019. *Cisplatin - Drug Information - Chemocare*. [online] Chemocare.com. Available at: http://chemocare.com/chemotherapy/drug-info/cisplatin.aspx [Accessed 21 Sep. 2019].

Cancer.Net. 2019. *Neuroblastoma - Childhood - Stages and Groups*. [online] Available at: https://www.cancer.net/cancer-types/neuroblastoma-childhood/stages-and-groups [Accessed 2 Mar. 2019].

Cancer.org. 2019. *What Is Neuroblastoma?*. [online] Available at: https://www.cancer.org/cancer/neuroblastoma/about/what-is-neuroblastoma.html [Accessed 2 Mar. 2019].

Cancer.org. 2022. *Neuroblastoma Stages and Prognostic Markers*. [online] Available at: <https://www.cancer.org/cancer/neuroblastoma/detection-diagnosis-staging/staging.html> [Accessed 13 May 2022].

Cancer.org. 2022. *Neuroblastoma Survival Rates | American Cancer Society*. [online] Available at: <https://www.cancer.org/cancer/neuroblastoma/detection-diagnosis-staging/survival-rates.html> [Accessed 4 May 2022].

Cancerresearchuk.org. 2019. *Doxorubicin (Adriamycin) | Cancer drugs | Cancer Research UK*. [online] Available at: https://www.cancerresearchuk.org/about-cancer/cancer-in-general/treatment/cancer-drugs/drugs/doxorubicin [Accessed 21 Sep. 2019].

Cavallo, F., De Giovanni, C., Nanni, P., Forni, G. and Lollini, P.L., 2011. 2011: the immune hallmarks of cancer. *Cancer Immunology, Immunotherapy*, *60*, pp.319-326.

Challagundla, K.B., Wise, P.M., Neviani, P., Chava, H., Murtadha, M., Xu, T., Kennedy, R., Ivan, C., Zhang, X., Vannini, I. and Fanini, F., 2015. Exosome-mediated transfer of microRNAs within the tumor microenvironment and neuroblastoma resistance to chemotherapy. *Journal of the National Cancer Institute*, *107*(7), p.djv135.

Chatterjee, K., Zhang, J., Honbo, N. and Karliner, J.S., 2010. Doxorubicin cardiomyopathy. *Cardiology*, *115*(2), pp.155-162.

Chauhan, V.P., Boucher, Y., Ferrone, C.R., Roberge, S., Martin, J.D., Stylianopoulos, T., Bardeesy, N., DePinho, R.A., Padera, T.P., Munn, L.L. and Jain, R.K., 2014. Compression of pancreatic tumor blood vessels by hyaluronan is caused by solid stress and not interstitial fluid pressure. *Cancer cell*, *26*(1), pp.14-15.

Chen, Y., Ding, X., Zhang, Y., Natalia, A., Sun, X., Wang, Z. and Shao, H., 2018. Design and synthesis of magnetic nanoparticles for biomedical diagnostics. *Quantitative Imaging in Medicine and Surgery*, 8(9), pp.957-970.

Cheung, N. and Dyer, M., 2013. Neuroblastoma: developmental biology, cancer genomics and immunotherapy. *Nature Reviews Cancer*, 13(6), pp.397-411.

Corrie, P.G., 2008. Cytotoxic chemotherapy: clinical aspects. *Medicine*, *36*(1), pp.24-28.

Dai, Y.N., Li, P., Zhang, J.P., Wang, A.Q. and Wei, Q., 2008. A novel pH sensitive N-succinyl chitosan/alginate hydrogel bead for nifedipine delivery. *Biopharmaceutics & drug disposition*, *29*(3), pp.173-184.

De Bernardi, B., Mosseri, V., Rubie, H., Castel, V., Foot, A., Ladenstein, R., Laureys, G., Beck-Popovic, M., De Lacerda, A.F., Pearson, A.D.J. and De Kraker, J., 2008. Treatment of localised resectable neuroblastoma. Results of the LNESG1 study by the SIOP Europe Neuroblastoma Group. *British journal of cancer*, *99*(7), pp.1027-1033.

Denard, B., Jiang, S., Peng, Y. and Ye, J., 2018. CREB3L1 as a potential biomarker predicting response of triple negative breast cancer to doxorubicin-based chemotherapy. *BMC cancer*, *18*, pp.1-7.

Dupuy, B., Arien, A. and Minnot, A.P., 1994. FT-IR of membranes made with alginate/polylysine complexes. Variations with the mannuronic or guluronic content of the polysaccharides. *Artificial Cells, Blood Substitutes, and Biotechnology*, *22*(1), pp.71-82.

Fitzakerly, J., 2022. *Cell Cycle Specificity*. [online] D.umn.edu. Available at: <https://www.d.umn.edu/~jfitzake/Lectures/DMED/Antineoplastics/GeneralConcepts/CellCycleSpecificity.html> [Accessed 16 May 2022].

Forouzani-Moghaddam, M.J., Nabian, P., Gholami, A., Dehghanbaghi, N., Azizipanah, M., Jokar, K., Eslami, F., Kargarian, Z., Tamehri, M., Zare, N. and Heydari, S., 2018. A review of neuroblastoma: prevalence, diagnosis, related genetic factors, and treatment. *Iranian Journal of Pediatric Hematology and Oncology*, *8*(4), pp.237-246.

Freemerman, A., Johnson, A., Sacks, G., Milner, J., Kirk, E., Troester, M., Macintyre, A., Goraksha-Hicks, P., Rathmell, J. and Makowski, L., 2014. Metabolic Reprogramming of Macrophages. *Journal of Biological Chemistry*, 289(11), pp.7884-7896.

Gao, Y., Jin, B., Shen, W., Sinko, P.J., Xie, X., Zhang, H. and Jia, L., 2016. China and the United States—global partners, competitors and collaborators in nanotechnology development. *Nanomedicine: Nanotechnology, Biology and Medicine*, *12*(1), pp.13-19.

Gedik, G.K., Hoefnagel, C.A., Bais, E. and Valdés Olmos, R.A., 2008. 131 I-MIBG therapy in metastatic phaeochromocytoma and paraganglioma. *European journal of nuclear medicine and molecular imaging*, *35*, pp.725-733.

Gupta, M. and Ngan, Y. 2016. A comparison between liposomal and nonliposomal formulations of doxorubicin in the treatment of cancer: An updated review. *Archives of Pharmacy Practice*, 7(1), p.1.

Hadla, M., Palazzolo, S., Corona, G., Caligiuri, I., Canzonieri, V., Toffoli, G. and Rizzolio, F., 2016. Exosomes increase the therapeutic index of doxorubicin in breast and ovarian cancer mouse models. *Nanomedicine*, *11*(18), pp.2431-2441.

Hanahan, D. and Weinberg, R.A., 2011. Hallmarks of cancer: the next generation. *cell*, *144*(5), pp.646-674.

Henderson, T.O., Bhatia, S., Pinto, N., London, W.B., McGrady, P., Crotty, C., Sun, C.L. and Cohn, S.L., 2011. Racial and ethnic disparities in risk and survival in children with neuroblastoma: a Children's Oncology Group study. *Journal of clinical oncology*, *29*(1), p.76.

Hickman, J.A., 1992. Apoptosis induced by anticancer drugs. *Cancer and Metastasis Reviews*, *11*, pp.121-139.

Hochella, M.F., Spencer, M.G. and Jones, K.L., 2015. Nanotechnology: nature's gift or scientists' brainchild?. *Environmental Science: Nano*, *2*(2), pp.114-119.

Iravani, S., 2011. Green synthesis of metal nanoparticles using plants. *Green Chemistry*, *13*(10), pp.2638-2650.

Jain, R.K., 2012. Delivery of molecular and cellular medicine to solid tumors. *Advanced drug delivery reviews*, *64*, pp.353-365.

Jemal, A., Bray, F., Forman, D., O'Brien, M., Ferlay, J., Center, M. and Parkin, D.M., 2012. Cancer burden in Africa and opportunities for prevention. *Cancer*, *118*(18), pp.4372-4384.

Johnsen, J.I., Dyberg, C. and Wickström, M., 2019. Neuroblastoma—A neural crest derived embryonal malignancy. *Frontiers in molecular neuroscience*, *12*, p.9.

Joko-Fru, W.Y., Jedy-Agba, E., Korir, A., Ogunbiyi, O., Dzamalala, C.P., Chokunonga, E., Wabinga, H., Manraj, S., Finesse, A., Somdyala, N. and Liu, B., 2020. The evolving epidemic of breast cancer

in sub-Saharan Africa: Results from the African Cancer Registry Network. *International Journal of Cancer*, *147*(8), pp.2131-2141.

Joo, W.D., Visintin, I. and Mor, G., 2013. Targeted cancer therapy–are the days of systemic chemotherapy numbered?. *Maturitas*, *76*(4), pp.308-314.

Karaman, D.Ş., Sarparanta, M.P., Rosenholm, J.M. and Airaksinen, A.J., 2018. Multimodality imaging of silica and silicon materials *in vivo*. *Advanced materials*, *30*(24), p.1703651.

Kargozar, S. and Mozafari, M., 2018. Nanotechnology and Nanomedicine: Start small, think big. *Materials Today: Proceedings*, *5*(7), pp.15492-15500.

Katuwavila, N.P., Perera, A.D.L., Samarakoon, S.R., Soysa, P., Karunaratne, V., Amaratunga, G.A. and Karunaratne, D., 2016. Chitosan-alginate nanoparticle system efficiently delivers doxorubicin to MCF-7 cells. *Journal of nanomaterials*, *2016*.

Khan, F.A., 2020. Nanomaterials: types, classifications, and sources. *Applications of nanomaterials in human health*, pp.1-13.

Khan, I., Saeed, K. and Khan, I., 2019. Nanoparticles: Properties, applications and toxicities. *Arabian Journal of Chemistry*, 12(7), pp.908-931.

Kong, G., Braun, R.D. and Dewhirst, M.W., 2000. Hyperthermia enables tumor-specific nanoparticle delivery: effect of particle size. *Cancer research*, *60*(16), pp.4440-4445.

Kost, J. and Langer, R., 2012. Responsive polymeric delivery systems. *Advanced drug delivery reviews*, *64*, pp.327-341.

Kumar, S., Chauhan, N., Gopal, M., Kumar, R. and Dilbaghi, N., 2015. Development and evaluation of alginate–chitosan nanocapsules for controlled release of acetamiprid. *International Journal of Biological Macromolecules*, 81, pp.631-637.

Kurapati, R. and Raichur, A.M., 2012. Graphene oxide based multilayer capsules with unique permeability properties: facile encapsulation of multiple drugs. *Chemical Communications*, *48*(48), pp.6013-6015.

Laprie, A., Michon, J., Hartmann, O., Munzer, C., Leclair, M.D., Coze, C., Valteau-Couanet, D., Plantaz, D., Carrie, C., Habrand, J.L. and Bergeron, C., 2004. High-dose chemotherapy followed by locoregional irradiation improves the outcome of patients with international neuroblastoma staging system Stage II and III neuroblastoma with MYCN amplification. *Cancer*, *101*(5), pp.1081-1089.

Lgcstandards.com., 2022. *LGC Standards*. [online] Available at: <https://www.lgcstandards.com/> [Accessed 3 August 2022].

Liu, C., Liu, F., Feng, L., Li, M., Zhang, J. and Zhang, N., 2013. The targeted co-delivery of DNA and doxorubicin to tumor cells via multifunctional PEI-PEG based nanoparticles. *Biomaterials*, *34*(10), pp.2547-2564.

Louis, C. and Shohet, J., 2015. Neuroblastoma: Molecular Pathogenesis and Therapy. *Annual Review of Medicine*, 66(1), pp.49-63.

Maeda, H., Wu, J., Sawa, T., Matsumura, Y. and Hori, K., 2000. Tumor vascular permeability and the EPR effect in macromolecular therapeutics: a review. *Journal of controlled release*, *65*(1-2), pp.271-284.

Maity, S., Mukhopadhyay, P., Kundu, P.P. and Chakraborti, A.S., 2017. Alginate coated chitosan core-shell nanoparticles for efficient oral delivery of naringenin in diabetic animals—An *in vitro* and *in vivo* approach. *Carbohydrate polymers*, *170*, pp.124-132.

Malatesta, M., 2021. Transmission electron microscopy as a powerful tool to investigate the interaction of nanoparticles with subcellular structures. *International Journal of Molecular Sciences*, *22*(23), p.12789.

Malis, J., 2013. Clinical Presentation of Neuroblastoma. Neuroblastoma. *InTech*. DOI: 10.5772/55921..

Maris, J., 2010. Recent Advances in Neuroblastoma. *New England Journal of Medicine*, 362(23), pp.2202-2211.

Michaelis, M., Bliss, J., Arnold, S., Hinsch, N., Rothweiler, F., Deubzer, H., Witt, O., Langer, K., Doerr, H., Wels, W. and Cinatl, J., 2008. Cisplatin-Resistant Neuroblastoma Cells Express Enhanced Levels of Epidermal Growth Factor Receptor (EGFR) and Are Sensitive to Treatment with EGFR-Specific Toxins. *Clinical Cancer Research*, 14(20), pp.6531-6537.

Mitra, S., Gaur, U., Ghosh, P. and Maitra, A., 2001. Tumour targeted delivery of encapsulated dextran–doxorubicin conjugate using chitosan nanoparticles as carrier. *Journal of Controlled Release*, 74(1-3), pp.317-323.

Mladenovska, K., Cruaud, O., Richomme, P., Belamie, E., Raicki, R., Venierjulienne, M., Popovski, E., Benoit, J. and Goracinova, K., 2007. 5-ASA loaded chitosan–Ca–alginate microparticles: Preparation and physicochemical characterization. *International Journal of Pharmaceutics*, 345(1-2), pp.59-69.

Mokhtari, R., Homayouni, T., Baluch, N., Morgatskaya, E., Kumar, S., Das, B. and Yeger, H., 2017. Combination therapy in combating cancer. *Oncotarget*, 8(23).

Mossé, Y., Laudenslager, M., Longo, L., Cole, K., Wood, A., Attiyeh, E., Laquaglia, M., Sennett, R., Lynch, J., Perri, P., Laureys, G., Speleman, F., Kim, C., Hou, C., Hakonarson, H., Torkamani, A., Schork, N., Brodeur, G., Tonini, G., Rappaport, E., Devoto, M. and Maris, J., 2008. Identification of ALK as a major familial neuroblastoma predisposition gene. *Nature*, 455(7215), pp.930-935.

Mukhopadhyay, P., Chakraborty, S., Bhattacharya, S., Mishra, R. and Kundu, P., 2015. pH-sensitive chitosan/alginate core-shell nanoparticles for efficient and safe oral insulin delivery. *International Journal of Biological Macromolecules*, 72, pp.640-648.

Mullassery, D., Losty P.D., 2016. Neuroblastoma. *Paediatrics and Child Health* 2016;26(2):68-72.

Munung, N., Ambele, M. and Moela, P., 2021. Advancing global equity in cancer genomics – challenges and opportunities in Sub-Saharan Africa. *Current Opinion in Genetics & Development*, 66, pp.20-24.

Nakagawara, A., 2004. Neural crest development and neuroblastoma: the genetic and biological link. *Progress in Brain Research*, pp.231-242.

Nalluri, S., Peirce, S., Tanos, R., Abdella, H., Karmali, D., Hogarty, M. and Goldsmith, K., 2015. EGFR signaling defines Mcl-1 survival dependency in neuroblastoma. *Cancer Biology & Therapy*, 16(2), pp.276-286.

Namkaew, J., Jaroonwitchawan, T., Rujanapun, N., Saelee, J. and Noisa, P., 2018. Combined effects of curcumin and doxorubicin on cell death and cell migration of SH-SY5Y human neuroblastoma cells. *In Vitro Cellular & Developmental Biology-Animal*, *54*, pp.629-639.

National Nanotechnology Initiative., 2022. *What Is Nanotechnology? | National Nanotechnology Initiative*. [online] Nano.gov. Available at: <https://www.nano.gov/nanotech-101/what/definition> [Accessed 25 May 2022].

Nia, H., Munn, L. and Jain, R., 2020. Physical traits of cancer. *Science*, 370(6516), p.eaaz0868.

Nie, S., Xing, Y., Kim, G. and Simons, J., 2007. Nanotechnology Applications in Cancer. *Annual Review of Biomedical Engineering*, 9(1), pp.257-288.

Ortega, J., Krailo, M., Haas, J., King, D., Ablin, A., Quinn, J., Feusner, J., Campbell, J., Lloyd, D. and Cherlow, J., 1991. Effective treatment of unresectable or metastatic hepatoblastoma with cisplatin and continuous infusion doxorubicin chemotherapy: a report from the Childrens Cancer Study Group. *Journal of Clinical Oncology*, 9(12), pp.2167-2176.

Pan, Y., Li, Y., Zhao, H., Zheng, J., Xu, H., Wei, G., Hao, J. and Cui, F., 2002. Bioadhesive polysaccharide in protein delivery system: chitosan nanoparticles improve the intestinal absorption of insulin *in vivo*. *International Journal of Pharmaceutics*, 249(1-2), pp.139-147.

Patil, J., Marapur, S., Kamalapur, M. and Shiralshetti, S., 2011. Ionotropically gelled novel hydrogel beads: Preparation, characterization and *in vitro* evaluation. *Indian Journal of Pharmaceutical Sciences*, 73(5), p.504.

Pedroso-Santana, S. and Fleitas-Salazar, N., 2020. Ionotropic gelation method in the synthesis of nanoparticles/microparticles for biomedical purposes. *Polymer International*, 69(5), pp.443-447.

Pilco-Ferreto, N. and Calaf, G.M., 2016. Influence of doxorubicin on apoptosis and oxidative stress in breast cancer cell lines. *International journal of oncology*, *49*(2), pp.753-762.

Pilleron, S., Soerjomataram, I., Charvat, H., Chokunonga, E., Somdyala, N., Wabinga, H., Korir, A., Bray, F., Jemal, A. and Maxwell Parkin, D., 2019. Cancer incidence in older adults in selected regions of sub-Saharan Africa, 2008–2012. *International Journal of Cancer*, 144(8), pp.1824-1833.

Pranatharthiharan, S., Patel, M., Malshe, V., Pujari, V., Gorakshakar, A., Madkaikar, M., Ghosh, K. and Devarajan, P., 2017. Asialoglycoprotein receptor targeted delivery of doxorubicin nanoparticles for hepatocellular carcinoma. *Drug Delivery*, 24(1), pp.20-29.

Rafiee, A., Alimohammadian, M.H., Gazori, T., Riazi-rad, F., Fatemi, S.M.R., Parizadeh, A., Haririan, I. and Havaskary, M., 2014. Comparison of chitosan, alginate and chitosan/alginate nanoparticles with respect to their size, stability, toxicity and transfection. *Asian Pacific Journal of Tropical Disease*, *4*(5), pp.372-377.

Raval, S., Singh, R., Joshi, D., Patel, H. and Mody, S., 2016. Recent developments in receptor tyrosine kinases targeted anticancer therapy. *Veterinary World*, 9(1), pp.80-90.

Ravi Kumar, M., Blanco-Prieto, M. and Waterhouse, D., 2013. Nanotheraputics. *Cancer Letters*, 334(2), pp.155-156.

Rebbaa, A., Chou, P. and Mirkin, B., 2001. Factors Secreted by Human Neuroblastoma Mediate Doxorubicin Resistance by Activating STAT3 and Inhibiting Apoptosis. *Molecular Medicine*, 7(6), pp.393-400.

Rebbaa, A., Zheng, X., Chou, P. and Mirkin, B., 2003. Caspase inhibition switches doxorubicin-induced apoptosis to senescence. *Oncogene*, 22(18), pp.2805-2811.

Rivankar, S., 2014. An overview of doxorubicin formulations in cancer therapy. *Journal of Cancer Research and Therapeutics*, 10(4), p.853.

Rizwanullah, M., Alam, M., Harshita, M., Mir, S., Rizvi, M. and Amin, S., 2020. Polymer-Lipid Hybrid Nanoparticles: A Next-Generation Nanocarrier for Targeted Treatment of Solid Tumors. *Current Pharmaceutical Design*, 26(11), pp.1206-1215.

Rodríguez-Nogales, C., Noguera, R., Couvreur, P. and Blanco-Prieto, M., 2019. Therapeutic Opportunities in Neuroblastoma Using Nanotechnology. *Journal of Pharmacology and Experimental Therapeutics*, 370(3), pp.625-635.

Salvioni, L., Rizzuto, M., Bertolini, J., Pandolfi, L., Colombo, M. and Prosperi, D., 2019. Thirty Years of Cancer Nanomedicine: Success, Frustration, and Hope. *Cancers*, 11(12), p.1855.

Schirrmacher, V., 2019. From chemotherapy to biological therapy: A review of novel concepts to reduce the side effects of systemic cancer treatment (Review). International Journal of Oncology, 54, 407-419. https://doi.org/10.3892/ijo.2018.4661

Schroeder, A., Kost, J. and Barenholz, Y., 2009. Ultrasound, liposomes, and drug delivery: principles for using ultrasound to control the release of drugs from liposomes. *Chemistry and Physics of Lipids*, 162(1-2), pp.1-16.

Seano, G., Nia, H.T., Emblem, K.E., Datta, M., Ren, J., Krishnan, S., Kloepper, J., Pinho, M.C., Ho, W.W., Ghosh, M. and Askoxylakis, V., 2019. Solid stress in brain tumours causes neuronal loss and neurological dysfunction and can be reversed by lithium. *Nature biomedical engineering*, *3*(3), pp.230-245.

Shojaei-Brosseau, T., Chompret, A., Abel, A., de Vathaire, F., Raquin, M., Brugières, L., Feunteun, J., Hartmann, O. and Bonaïti-Pellié, C., 2003. Genetic epidemiology of neuroblastoma: A study of

426 cases at the Institut Gustave-Roussy in France. *Pediatric Blood & Cancer*, 42(1), pp.99-105.

Smith, D.J., 2015. Characterization of nanomaterials using transmission electron microscopy. pp.1-29.

Song, W., Su, X., Gregory, D., Li, W., Cai, Z. and Zhao, X., 2018. Magnetic Alginate/Chitosan Nanoparticles for Targeted Delivery of Curcumin into Human Breast Cancer Cells. *Nanomaterials*, 8(11), p.907.

South African National Nanotechnology Strategy., 2022. [online] Gov.za. Available at: <https://www.gov.za/sites/default/files/gcis_document/201409/dstnanotech180120060.pdf> [Accessed 26 May 2022].

Sritharan, S. and Sivalingam, N., 2021. A comprehensive review on time-tested anticancer drug doxorubicin. *Life Sciences*, 278, p.119527.

Strober, W., Trypan blue exclusion test of cell viability; 2001. *Current protocols in immunology*, *21*.

Swift, C., Eklund, M., Kraveka, J. and Alazraki, A., 2018. Updates in Diagnosis, Management, and Treatment of Neuroblastoma. *RadioGraphics*, 38(2), pp.566-580.

Tsubota, S. Kadomatsu, K., 2017. Origin and Mechanism of Neuroblastoma. *Oncoscinece* **4**, 7-8. [online] Available at: https://www.ncbi.nlm.nih.gov/pmc/articles/PMC5616197/ [Accessed: 2 March 2019].

Verma, A.K., Leekha, A., Kumar, V., Moin, I. and Kumar, S., 2018. Biodistribution and *In-vivo* efficacy of doxorubicin loaded chitosan nanoparticles in Ehrlich Ascites Carcinoma (EAC) bearing Balb/C mice. *J. Nanomed. Nanotechnol*, *9*, p.510.

Visualsonline.cancer.gov., 2019. *Five-Year Survival Rate for Selected Cancers Among Children: Image Details - NCI Visuals Online*. [online] Available at: https://visualsonline.cancer.gov/details.cfm?cid=eb_govdel&imageid=12055 [Accessed 2 Mar. 2019].

Von Hoff, D., 1979. Risk Factors for Doxorubicin-lnduced Congestive Heart Failure. *Annals of Internal Medicine*, 91(5), p.710.

Weinstein, J., Katzenstein, H. and Cohn, S., 2003. Advances in the Diagnosis and Treatment of Neuroblastoma. *The Oncologist*, 8(3), pp.278-292.

Whittle, S., Smith, V., Doherty, E., Zhao, S., McCarty, S. and Zage, P., 2017. Overview and recent advances in the treatment of neuroblastoma. *Expert Review of Anticancer Therapy*, 17(4), pp.369-386.

Wu, T., Yu, S., Lin, D., Wu, Z., Xu, J., Zhang, J., Ding, Z., Miao, Y., Liu, T., Chen, T. and Cai, X., 2020. Preparation, characterization, and release behavior of doxorubicin hydrochloride from dual cross-linked chitosan/alginate hydrogel beads. *ACS Applied Bio Materials*, *3*(5), pp.3057-3065.

Wuang, S., Neoh, K., Kang, E., Leckband, D. and Pack, D., 2011. Acid-sensitive magnetic nanoparticles as potential drug depots. *AIChE Journal*, 57(6), pp.1638-1645.

Yap, T.A., Omlin, A. and De Bono, J.S., 2013. Development of therapeutic combinations targeting major cancer signaling pathways. *Journal of Clinical Oncology*, *31*(12), pp.1592-1605.

Yoncheva, K., Tzankov, B., Yordanov, Y., Spassova, I., Kovacheva, D., Frosini, M., Valoti, M. and Tzankova, V., 2020. Encapsulation of doxorubicin in chitosan-alginate nanoparticles improves its stability and cytotoxicity in resistant lymphoma L5178 MDR cells. *Journal of Drug Delivery Science and Technology*, *59*, p.101870.

Yuan, F., Dellian, M., Fukumura, D., Leunig, M., Berk, D.A., Torchilin, V.P. and Jain, R.K., 1995 Vascular permeability in a human tumor xenograft: molecular size dependence and cutoff size. *Cancer research*, *55*(17), pp.3752-3756.

Zanini, C., Giribaldi, G., Mandili, G., Carta, F., Crescenzio, N., Bisaro, B., Doria, A., Foglia, L., di Montezemolo, L., Timeus, F. and Turrini, F., 2007. Inhibition of heat shock proteins (HSP)

expression by quercetin and differential doxorubicin sensitization in neuroblastoma and Ewing's sarcoma cell lines. *Journal of Neurochemistry*, 103(4), pp.1344-1354.

Zhang, Y., Yang, C., Wang, W., Liu, J., Liu, Q., Huang, F., Chu, L., Gao, H., Li, C., Kong, D., Liu, Q. and Liu, J., 2016. Co-delivery of doxorubicin and curcumin by pH-sensitive prodrug nanoparticle for combination therapy of cancer. *Scientific Reports*, 6(1).

Zhao, N., C Woodle, M. and Mixson, A., 2018. Advances in Delivery Systems for Doxorubicin. *Journal of Nanomedicine & Nanotechnology*, 09(05)

Appendix 1

TEM of a Similar Nanoparticle Drug Delivery System

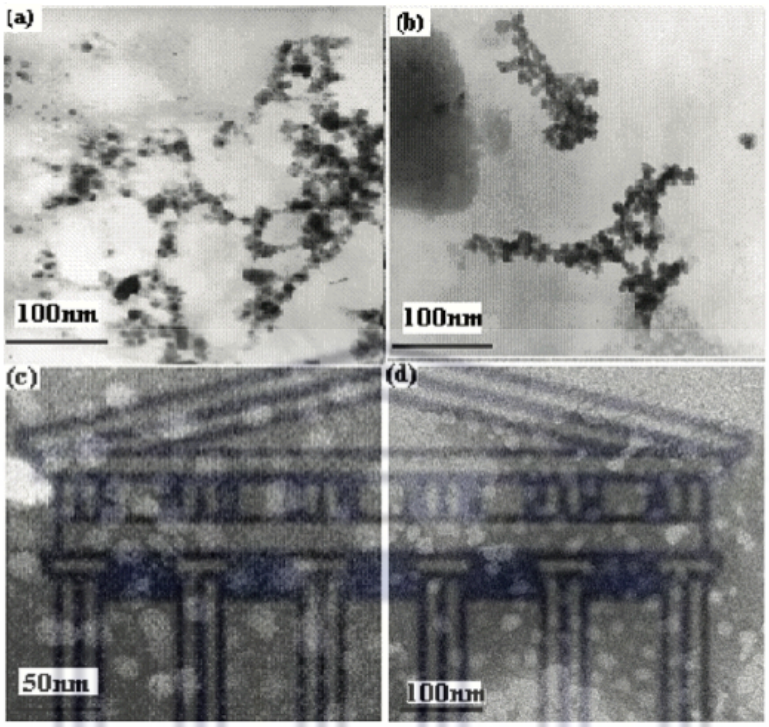

Figure 1.1: TEM of nifedipine loaded CS-ALG nanoparticles. Magnification (a x60000); (b x60000); (c x 600000); (d x 300000). Reproduced from Dai et al., (2008).

Appendix 2

Doxorubicin-induced Apoptosis and Senescence

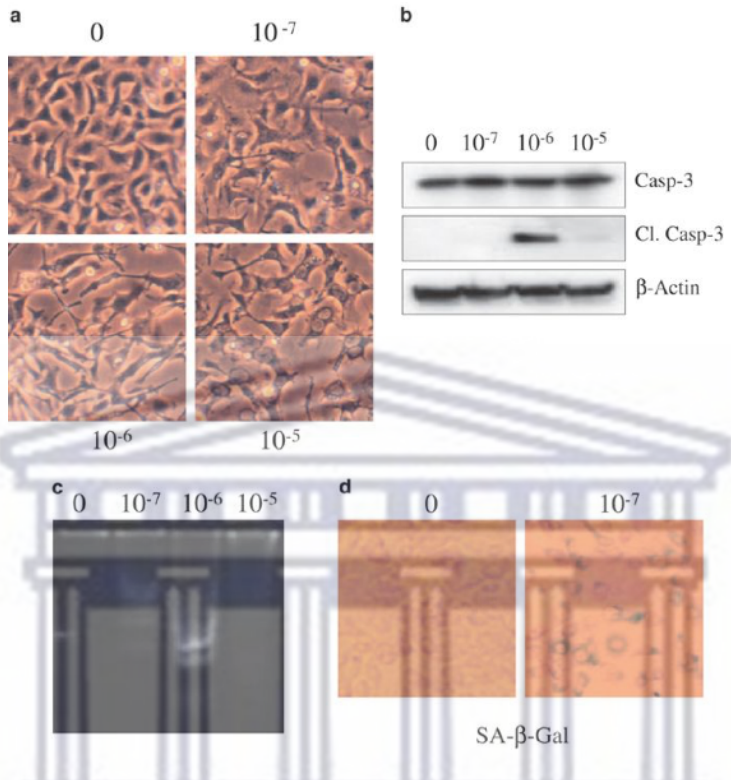

Figure 2.1: Cellular morphology following exposure to doxorubicin. Reproduced from Rebbaa, A., Zheng, X., Chou, P. and Mirkin, B. (2003). Caspase inhibition switches doxorubicin-induced apoptosis to senescence. *Oncogene*, 22(18), pp.2805-2811.

Appendix 3

Passive and Active Targeting of Cancer Cells Using Nanoparticles

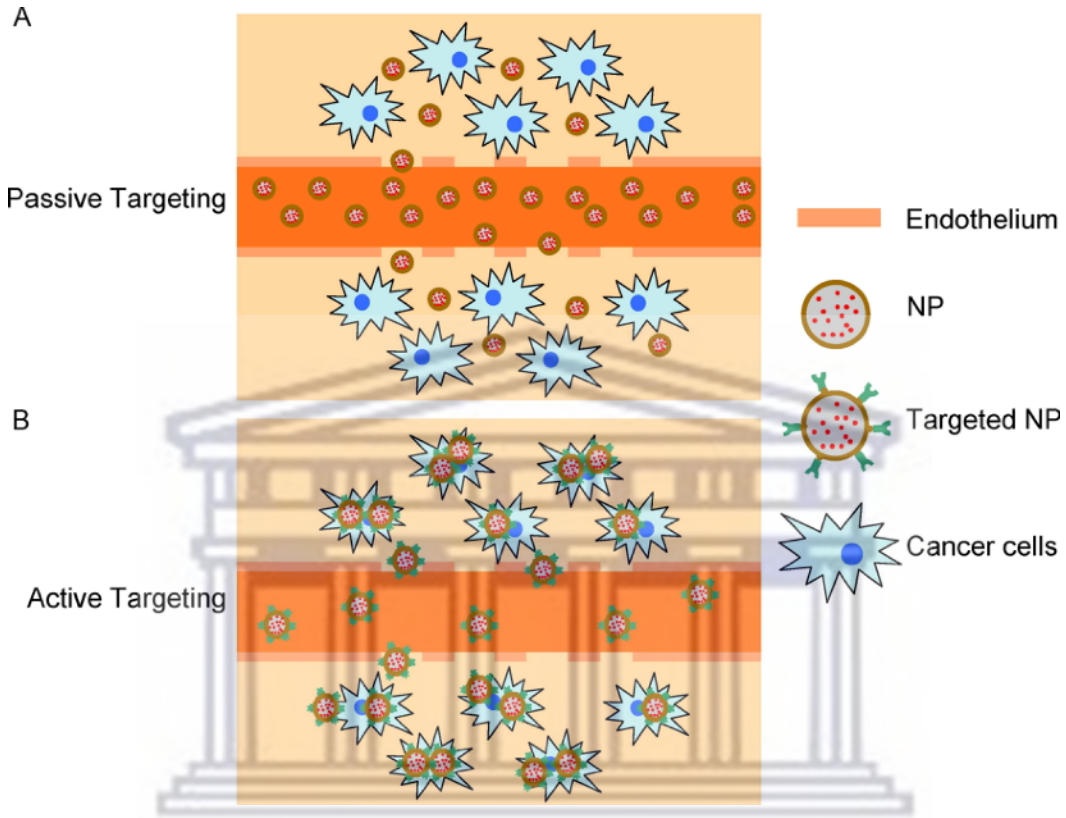

Figure 3.1: Schematic illustration of nanoparticle targeting. **(A)** Nanoparticles are concentrated in the tumor interstitium via passive extravasation through the leaky microvasculature shown as gaps in the endothelial layer (light orange). This process has been named the EPR effect. In this case the efficacy of nanoparticles is largely mediated through the local release of the drug near the cancer cells. (B) Targeted nanoparticles similarly concentrate in the tumor interstitium through the EPR effect but once there, nanoparticles are actively taken up by cancer cells after binding to their target antigens on the surface of the cancer cells. In this case the drugs are released largely inside the cancer cells resulting in enhanced efficacy. Reproduced from **Alexis, F. *et al.* (2008) "New frontiers in nanotechnology for cancer treatment," *Urologic Oncology: Seminars and Original Investigations*, 26(1), pp. 74–85. Available at: https://doi.org/10.1016/j.urolonc.2007.03.017.**